REPORT NO. NADC-89090-60

FATIGUE BEHAVIOR OF P/M 7091 AND I/M 7475 ALUMINUM ALLOYS

Eun U. Lee
Air Vehicle and Crew Systems Technology Department (Code 6063)
NAVAL AIR DEVELOPMENT CENTER
Warminster, PA 18974-5000

1 OCTOBER 1989

PHASE REPORT
Project No. AO6

Prepared for
Air Vehicle and Crew Systems Technology Department (Code 606)
NAVAL AIR DEVELOPMENT CENTER
Warminster, PA 18974-5000

NOTICES

REPORT NUMBERING SYSTEM — The numbering of technical project reports issued by the Naval Air Development Center is arranged for specific identification purposes. Each number consists of the Center acronym, the calendar year in which the number was assigned, the sequence number of the report within the specific calendar year, and the official 2-digit correspondence code of the Command Officer or the Functional Department responsible for the report. For example: Report No. NADC-88020-60 indicates the twentieth Center report for the year 1988 and prepared by the Air Vehicle and Crew Systems Technology Department. The numerical codes are as follows:

CODE	OFFICE OR DEPARTMENT
00	Commander, Naval Air Development Center
01	Technical Director, Naval Air Development Center
05	Computer Department
10	AntiSubmarine Warfare Systems Department
20	Tactical Air Systems Department
30	Warfare Systems Analysis Department
40	Communication Navigation Technology Department
50	Mission Avionics Technology Department
60	Air Vehicle & Crew Systems Technology Department
70	Systems & Software Technology Department
80	Engineering Support Group
90	Test & Evaluation Group

PRODUCT ENDORSEMENT — The discussion or instructions concerning commercial products herein do not constitute an endorsement by the Government nor do they convey or imply the license or right to use such products.

Reviewed By: J Waldman **Date:** 3/20/90
Branch Head

Reviewed By: J. [illegible] **Date:** 3/24/90
Division Head

Reviewed By: W. L. Morris **Date:** 3/27/90
Director/Deputy Director

UNCLASSIFIED
SECURITY CLASSIFICATION OF THIS PAGE

REPORT DOCUMENTATION PAGE

Form Approved OMB No. 0704-0188

1a. REPORT SECURITY CLASSIFICATION: Unclassified

1b. RESTRICTIVE MARKINGS:

2a. SECURITY CLASSIFICATION AUTHORITY:

2b. DECLASSIFICATION / DOWNGRADING SCHEDULE:

3. DISTRIBUTION / AVAILABILITY OF REPORT: Approved for Public Release; Distribution is Unlimited

4. PERFORMING ORGANIZATION REPORT NUMBER(S): NADC 89090-60

5. MONITORING ORGANIZATION REPORT NUMBER(S):

6a. NAME OF PERFORMING ORGANIZATION: Aircraft and Crew Systems Technology Department

6b. OFFICE SYMBOL (If applicable): 6063

7a. NAME OF MONITORING ORGANIZATION:

6c. ADDRESS (City, State, and ZIP Code): NAVAL AIR DEVELOPMENT CENTER Warminster, PA 18974-5000

7b. ADDRESS (City, State, and ZIP Code):

8a. NAME OF FUNDING / SPONSORING ORGANIZATION: Aircraft and Crew Systems Technology Department

8b. OFFICE SYMBOL (If applicable): 606

9. PROCUREMENT INSTRUMENT IDENTIFICATION NUMBER:

8c. ADDRESS (City, State, and ZIP Code): NAVAL AIR DEVELOPMENT CENTER Warminster, PA 18974-5000

10. SOURCE OF FUNDING NUMBERS

PROGRAM ELEMENT NO.	PROJECT NO.	TASK NO.	WORK UNIT ACCESSION NO.
	A06		

11. TITLE (Include Security Classification): Fatique Behavior of P/M 7091 and I/M 7475 Aluminum Alloys

12. PERSONAL AUTHOR(S): Eun U. Lee

13a. TYPE OF REPORT	13b. TIME COVERED	14. DATE OF REPORT (Year, Month, Day)	15. PAGE COUNT
Phase	FROM _____ TO _____	1989 October 1	

16. SUPPLEMENTARY NOTATION:

17. COSATI CODES			18. SUBJECT TERMS (Continue on reverse if necessary and identify by block number)
FIELD	GROUP	SUB-GROUP	P/M 7091-T7E69 Aluminum Alloy, FALSTAFF, Spectrum Loading
			I/M 7475-T7351 Aluminum Alloy, MINI-TWIST, Crack Jump

19. ABSTRACT (Continue on reverse if necessary and identify by block number)

The fatigue behaviors, tensile properties, microstructures, and fractographic features of P/M 7091-T7E69 and I/M 7475-T7351 aluminum alloys were studied and compared. In this study, the fatigue tests were performed under constant amplitude and FALSTAFF and MINI-TWIST spectrum loadings.

The P/M 7091-T7E69 aluminum alloy has greater tensile strength but lower fracture toughness than the I/M 7475-T7351 aluminum alloy. The dominant microstructure difference between these two alloys is the extra phases in P/M 7091-T7E69 aluminum alloy: Co_2Al_9 or $[Co, Fe]_2Al_9$ spheroids and numerous oxide particles along prior powder boundaries (PPB) as well as within the powders. The fatigue crack growth path is tortuous in the P/M 7091-T7E69 aluminum alloy but straight in the I/M 7475-T7351 aluminum alloy. The crack path tortuousness arises from frequent crack deflections

20. DISTRIBUTION / AVAILABILITY OF ABSTRACT: ☒ UNCLASSIFIED / UNLIMITED ☐ SAME AS RPT. ☐ DTIC USERS

21. ABSTRACT SECURITY CLASSIFICATION: Unclassified

22a. NAME OF RESPONSIBLE INDIVIDUAL: Eun U. Lee

22b. TELEPHONE (Include Area Code): (215) 441-1663

22c. OFFICE SYMBOL: 6063

DD Form 1473, JUN 86 — Previous editions are obsolete. — SECURITY CLASSIFICATION OF THIS PAGE

S/N 0102-LF-014-6603 — UNCLASSIFIED

BLOCK 19 continued

at PPB or grain boundaries (GB) and occasional crack growth along PPB or GB. Crack jumps occur in the P/M 7091-T7E69 aluminum alloy under fatigue loadings, except the constant-amplitude loading with R=0.1. They are induced by nucleation of microvoids at the numerous oxide particles and their growth and coalescence ahead of the advancing fatigue crack tip. The fatigue resistance of the P/M 7091-T7E69 aluminum alloy is inferior to that of the I/M 7475-T7351 aluminum alloy. This inferiority is even more unfavorable under the FALSTAFF and MINI-TWIST spectrum loading. The extremely poor fatigue resistance of the P/M 7091-T7E69 aluminum alloy is attributable to the extensive crack jumps.

CONTENTS

FIGURES

FIGURES (Cont'd)

TABLES

ACKNOWLEDGEMENTS

The author is grateful to Drs. J. Waldman and W. Scott for their constant encouragement and to Dr. R.J.H. Wanhill of the National Aerospace Laboratory, NLR, The Netherlands, for providing the specimen material (a P/M 7091-T7E69 aluminum alloy forging) and for helpful discussions. The author also thanks J.J. Minecci, V.J. Catone, and R.H. Dalrymple for computer analysis on aircraft loading spectrums; J. Cook for fatigue testing, W. Weist for SEM work, and H. Tyndall for TEM work.

INTRODUCTION

Powder metallurgy (P/M) processing produces a fine, uniform grain structure and a homogeneous distribution of alloying elements.[1] It also enables element additions not possible in ingot metallurgy (I/M) alloys because of ingot cracking and coarse segregation. As a result, P/M products are more isotropic with respect to strength and may have good fatigue crack initiation resistance.

Although the resistance of P/M aluminum alloys to fatigue crack growth has been investigated rather extensively,[2-10] it is still not generally understood well. The fatigue crack growth behavior of P/M aluminum alloys under constant-amplitude loading cannot always predict that under spectrum loading. Conclusions drawn from ranking P/M and I/M aluminum alloys based on constant-amplitude loading tests can be different from those based on spectrum loading tests, and at times these rankings can be reversed.[2] Some typical examples follow.

According to Wanhill[2] and Schra,[6] under constant-amplitude loading the fatigue crack growth (FCG) resistance of a P/M 7091-T7E69 aluminum alloy is equivalent to or better than that of I/M aluminum alloys 7010-T736, 7050-T736, 7075-T73, and 7175-T736. Under spectrum loading, however, the P/M aluminum alloy is greatly inferior. Rafalin's investigation[7] shows that under constant-amplitude loading the FCG rates of a P/M CT-91 aluminum alloy are lower than those of an I/M 7475-T6150 aluminum alloy. This behavior is reversed at low stress intensity factor range ΔK levels. On the other hand, Hart[8] indicates that under constant-amplitude loading FCG rates of a P/M X7091-T7E69 aluminum alloy are generally faster than those of an I/M 7075-T7351 aluminum alloy at intermediate ΔK levels of 2.7 to 10 ksi$\sqrt{\text{in}}$. At low ΔK levels below 2.7 ksi$\sqrt{\text{in}}$, the FCG rates of P/M aluminum alloy are comparable to those of I/M aluminum alloy. Similarly, Ruschau[9] reports that the constant-amplitude FCG rates of P/M 7091-T7E69 aluminum alloy are considerably greater than those of I/M 7050-T76 aluminum alloy. But under spectrum loading the P/M aluminum alloy is consistently superior to the I/M aluminum alloy in relation to FCG resistance. Bretz[10] also points out that the spectrum fatigue life of

P/M 7091-T7E69 aluminum alloy can be nearly three times longer than comparable conventional aluminum alloys in the 7XXX series (7050-T6510, 7050-T7E63, and 7475-T7351).

To understand the fatigue crack growth resistance of P/M aluminum alloys, the fatigue behaviors of P/M 7091-T7E69 and I/M 7475-T7351 aluminum alloys are investigated and compared under constant-amplitude and spectrum loadings in this study. The constant-amplitude fatigue test aims at establishing the baseline fatigue data, while the spectrum loading fatigue test determines the response of the alloys to realistic load sequences for fighter and transport aircrafts.

EXPERIMENTAL PROCEDURE

MATERIAL AND SPECIMEN PREPARATION

Two aluminum alloys, P/M 7091-T7E69 die forging and I/M 7475-T7351 plate, were selected as the specimen materials, considering their similarity in chemical composition. Their chemical compositions are given in Table 1. The P/M 7091-T7E69 aluminum alloy die forging, Figure 1, was supplied by the National Aerospace Laboratory, NLR, The Netherlands. The positions of tensile and fatigue test specimens in this forging are shown in Figure 2, and the details of the specimens are given in Figures 3 and 4. The specimens of I/M 7475-T7351 aluminum alloy were prepared from a 12.7-mm-thick plate.

TENSILE AND FATIGUE TESTS

Both the tensile and fatigue tests were done on a closed-loop electro-hydraulic MTS system in a controlled-laboratory atmosphere of 75 degrees F and 45 percent relative humidity.

The tensile test was performed, using dogbone specimens, at a loading rate of 17,794 N/min (4000 lb/min).

The fatigue tests were carried out using center-cracked tension (CCT) specimens under constant-amplitude and aircraft spectrum loadings. The loadings were in the longitudinal (L) direction of the P/M 7091-T7E69 aluminum alloy die forging and in the original rolling (L) direction of the I/M 7475-T7351 aluminum alloy plate. In the constant-amplitude loading fatigue tests, the load waveform was haversine, the stress ratios ($R = \sigma_{min}/\sigma_{max}$) 0.1 and 0.5, and the frequency 10 Hz. For the aircraft spectrum loading fatigue tests, two spectrum sequences, Fighter Aircraft Loading STAndard For Fatigue (FALSTAFF) and shortened version of Transport Wing STandard (MINI-TWIST), were employed.

FALSTAFF was developed by the National Aerospace Laboratory, NLR, Laboratorium Für Betriebsfestigkeit (Darmstadt), Industrieanlagen-Betriebsgesellschaft (Ottobrunn), and the Eid-

genössisches Flugzeugwerk (Emmen).[11] The FALSTAFF sequence consists of blocks of 200 different flights classified into three groups of mission types:

- repetitive patterns of severe maneuvering
- severe maneuvering
- moderate maneuvering

The sequence of flights and flight loads is random. All peak and trough load values are classed into 32 equidistant, discrete levels. Level 1 is assigned to the lowest trough value, and level 32 is assigned to the highest peak value. The physical zero stress/load value is located at the level equivalent to 7.5269.

In this study the applied stress is 7 MPa per FALSTAFF level, resulting in a maximum stress level of 171.3 MPa and a minimum stress level of –45.7 MPa.

TWIST represents the load history of the wing root of transport aircraft, and it was established by the National Aerospace Laboratory, NLR, and Laboratorium Für Betriebsfestigkeit (Darmstadt).[12] MINI-TWIST[13] is a shortened version of TWIST, with 95 percent of the lowest load-amplitude cycles omitted. Since the omitted load cycles also contribute to damage, the test results with MINI-TWIST overestimate the fatigue life as compared with TWIST. However, the absolute fatigue lives are less important for alloy comparison; thus, MINI-TWIST serves the purpose of this study.

MINI-TWIST consists of blocks of 4000 different flights, which are classified into 10 types ranging from stormy to calm conditions. The spectrum, having initially ten load-amplitude levels, is truncated to the third-highest load-amplitude level in this study. It provides eight occurrences of the maximum stress level 126.5 MPa in a block of 4000 flights. This is a reasonable truncation level for crack growth tests. The minimum stress level is –16.5 MPa.

Both the FALSTAFF and MINI-TWIST sequences contain compression load cycles. Possible buckling during compression loading was prevented by a plastic sheet-lined aluminum alloy antibuckling guide with cutout to allow observation of the crack.

In every fatigue test, when the crack became visible on the polished specimen surface, the cyclic loading was stopped and the crack length was measured using a traveling microscope. This measurement was repeated until the crack tip reached an edge of the specimen or until the specimen was fractured. In the constant-amplitude fatigue test, the crack growth rate, da/dN, was determined by the seven-point incremental polynomial method.[14] (a = one half crack length, N = number of loading cycles.) The corresponding stress intensity factor range, ΔK, was calculated using the following equation.[14]

$$\Delta K = \frac{\Delta P}{B}\sqrt{\frac{\pi}{2}\cdot\frac{\alpha}{W}\cdot\sec\left(\frac{\pi\alpha}{2}\right)}$$

$$\alpha = \frac{2a}{W}$$

where

$\Delta P = P_{max} - P_{min}$ = applied load range

P_{max} = maximum applied load

P_{min} = minimum applied load

B = specimen thickness

W = specimen width

MICROSTRUCTURAL AND FRACTOGRAPHIC EXAMINATIONS

The microstructures of the specimens were studied with an optical microscope, a JEOL 100CX2 transmission electron microscope, and an AMR 1000 scanning electron microscope operated at accelerating voltages of 120 and 20 kV, respectively. For the optical microscopy and the scanning electron microscopy, the specimens were etched with Keller's reagent. The transmission electron microscopy foils were prepared by means of electro-polishing.

The fracture surface morphologies of the specimens were examined with an AMR 100 scanning electron microscope operated at an accelerating voltage of 20 kV.

RESULTS

The results of the study are divided into four parts: tensile properties, fatigue behavior, microstructure, and fractograph.

TENSILE PROPERTIES

Tensile test results of P/M 7091-T7E69 and I/M 7475-T7351 aluminum alloys are shown in Tables 2 and 3 and in Figure 5. The following aspects are indicated:

1. P/M 7091-T7E69 aluminum alloy has greater tensile yield strength and ultimate tensile strength than I/M 7475-T7351 aluminum alloy. The tensile yield strength superiority of P/M 7091-T7E69 aluminum alloy to I/M 7475-T7351 aluminum alloy is 19 percent for the L direction and 18 percent for the T direction. The ultimate tensile strength superiority is 12 percent for the L direction and 10 percent for the T direction.

2. P/M 7091-T7E69 aluminum alloy has less elongation than I/M 7475-T7351 aluminum alloy. The elongation inferiority of P/M 7091-T7E69 aluminum alloy to I/M 7475-T7351 aluminum alloy is 16 percent for the L direction and 38 percent for the T direction.

FATIGUE BEHAVIOR

Fatigue test results are separated into two sections: constant-amplitude loading fatigue and aircraft spectrum loading fatigue.

CONSTANT-AMPLITUDE LOADING FATIGUE

In I/M 7475-T7351 aluminum alloy specimens, the fatigue crack growth is regular in a plane normal to the loading axis, with only minor differences in the crack length at the left and right sides of the center hole, as shown in Figure 6(a).

In P/M 7091-T7E69 aluminum alloy specimens, however, the fatigue crack growth is quite irregular. The crack path is tortuous and deviates from the plane of symmetry; the differences between the left and right crack lengths are large, as shown in Figure 6(b). Therefore, the crack length projected in the plane of symmetry is taken instead of the actual one for the plot of half crack length versus number of fatigue loading cycles and that of crack growth rate versus stress intensity factor range.

The increasing crack length with increasing number of fatigue loading cycles; the variation of crack growth rate, da/dN, with stress intensity factor range, ΔK; and the fatigue crack growth life are shown in Figures 7 through 11 and Table 4. The following features are indicated:

1. The fatigue crack growth rate of P/M 7091-T7E69 aluminum alloy is greater than that of I/M 7475-T7351 aluminum alloy at the stress intensity factor ranges employed for both R = 0.1 and R = 0.5. For both alloys the fatigue crack growth rate is greater at a given stress intensity factor range with R = 0.5 than with R = 0.1.

2. The fatigue crack growth lives of P/M 7091-T7E69 aluminum alloy are shorter than those of I/M 7475-T7351 aluminum alloy in the tests with R= 0.1 and R = 0.5. The life ratios are 0.19 for R = 0.1 and 0.26 for R = 0.5, respectively.

From the foregoing it is evident that P/M 7091-T7E69 aluminum alloy is inferior to I/M 7475-T7351 aluminum alloy with respect to fatigue resistance under constant-amplitude loading.

AIRCRAFT SPECTRUM LOADING FATIGUE

Test results of aircraft spectrum loading fatigue are divided into two parts: FALSTAFF and MINI-TWIST spectrum loading fatigues.

1. FALSTAFF Spectrum Loading Fatigue

Fatigue crack growth life under FALSTAFF spectrum loading is shown in Figure 12 and Table 5, and the variation of crack length with number of flights is shown in Figure 13. The fatigue crack growth behavior of P/M 7091-T7E69 aluminum alloy is clearly inferior under the FALSTAFF spectrum loading. One of the P/M 7091-T7E69 aluminum alloy specimens fractured at 33 flights before any visible crack grew. The other failed when the crack grew only 2.9 mm from the notches at 143 flights. On the other hand, an I/M 7475-T7351 aluminum alloy specimen survived until the crack grew 62 mm from the notches at 7635 flights. The mean fatigue crack growth life of the P/M 7091-T7E69 aluminum alloy specimens is only 1 percent of that of the I/M 7475-T7351 aluminum alloy specimen.

2. MINI-TWIST Spectrum Loading Fatigue

Fatigue crack growth life under MINI-TWIST spectrum loading is also shown in Figure 12 and Table 5, and the variation of crack length with numbers of flights and blocks Is shown in Figure 14. The fatigue crack growth behavior of P/M 7091-T7E69 aluminum alloy is also very poor under MINI-TWIST spectrum loading. A P/M 7091-T7E69 aluminum alloy specimen fractured at 1465 flights after the crack grew only 7.2 mm from the notches. However, an I/M 7475-T7351 aluminum alloy specimen failed after the crack grew 73 mm from the notches at 31,350 flights. The fatigue crack growth life of the P/M 7091-T7E69 aluminum alloy specimen is 5 percent of that of the I/M 7475-T7351 aluminum alloy specimen.

MICROSTRUCTURE

A transmission electron micrograph (TEM) of P/M 7091-T7E69 aluminum alloy Is shown In Figure 15(a). The dominant microstructural features are prior powder boundaries (PPB) and small particles. The PPB are sharply defined by smooth powder surfaces contacting each other but are poorly defined by rough powder surfaces with broken surface oxides. Many of the particles are Co_2Al_9 or $[Co, Fe]_2Al_9$ and oxides.

The Co_2Al_9 or $[Co, Fe]_2Al_9$ particles appear as dark spheroids with diameters ranging from 30 to 70 nm. They are located on grain boundaries as well as within grains and do not appear to be deformed or fractured by prior forging. Oxide particles appear as dark particles somewhat lighter and much smaller than the Co_2Al_9 or $[Co, Fe]_2Al_9$ particles. They are present as dense arrays mostly along PPB and some inside powder. Their size ranges from 1 to 15 nm. For P/M alloys, an oxide film forms on the powder surface during air-atomization. Subsequent processing tends to rupture the oxide films, leaving arrays of oxide fragments on the boundaries and in the interior of powder. The oxide particles have been identified as amorphous Al_2O_3 and crystalline MgO.[15]

A transmission electron micrograph (TEM) of I/M 7475-T7351 aluminum alloy is given in Figure 15(b). Precipitated fine particles and platelets of $MgZn_2$ and large particles of $Cr_2Mg_3Al_{18}$ are visible. However, no oxide particles are detectable.

FRACTOGRAPHY

Representative fracture surfaces of the tensile test specimens are shown in Figure 16. The fracture planes of both the P/M 7091-T7E69 and I/M 7475-T7351 aluminum alloy specimens are slanted approximately 45 degrees to the tensile loading axis for LT and TL orientations. For ST orientation, however, the fracture plane of the P/M 7091-T7E69 aluminum alloy specimen is approximetely 90 degrees to the tensile loading axis. (No tensile test was done for the ST orientation of the I/M 7475-T7351 aluminum alloy specimen.)

These features indicate that fracture occurs by shear for the LT and TL orientations of specimens from both alloys, and that fracture occurs by tensile rupture for the P/M 7091-T7E69 aluminum alloy specimens of ST orientation.

The SEM fractographs of the tensile test specimens are contained in Figures 17 and 18. Those of the P/M 7091-T7E69 aluminum alloy specimens of LT and TL orientations show fine, fibrous structure

at low magnifications and have a "layered" appearance caused by sheets of dimples at higher magnifications (Figure 17). In many of the dimples small particles can be seen, Indicating nucleation of microvoids at arrays of particles. In the specimens of ST orientation, the fracture surface appears grainy at low magnifications and exhibits equiaxed dimples at higher magnifications. Many of these dimples contaln small particles, as shown in Figure 17. Fractographs of the I/M 7475-T7351 aluminum alloy specimens of LT and TL orientations are less fibrous and show larger dimples (Figure 18).

The crack planes of the P/M 7091-T7E69 aluminum alloy fatigue test specimens change their orientations frequently during fatigue crack growth. The change of crack plane orientation is most distinct In the fatigue loading of MINI-TWIST, foliowed by diminishing tortuosity in the order of FALSTAFF, constant amplitude with R = 0.5, and constant amplitude with R = 0.1. Conversely, the crack planes of the I/M 7475-T7351 aluminum alloy fatigue test specimens remain perpendicular to the fatigue loading axis throughout the fatigue crack growth life.

Representative fracture surfaces of the fatigue test specimens are illustrated in Figures 19 through 22. Each fracture surface consists of areas of slow crack growth and overload fracture. The fracture surfaces of the P/M 7091-T7E69 aluminum alloy specimens are finer than those of the I/M 7475-T7351 aluminum alloy specimens for both slow crack growth and overload fracture. For the P/M 7091-T7E69 aluminum alloy specimens the slow crack growth area is a mixture of bright beach mark zones of fatigue crack growth and darker zones of crack jump, except for constant-amplitude loading with R = 0.1. (In SEM fractographs, the beach mark zones are dark and the crack jump zones are lighter.) Crack jumping Is particularly predominant during the FALSTAFF and MINI-TWIST spectrum loadings.

The SEM fractographs of the fatigue test specimens are contained in Figures 23 through 30. Those of the P/M 7091-T7E69 aluminum alloy specimens, which were fatigue-tested under constant-amplitude loadings of R = 0.1 and 0.5 (Figures 23 and 24), exhibit the following:

1. In the beach mark zone near the notch (or the fatigue crack initiation site), facets can be seen. Some facets contain river patterns and faint striations. Nearly parallel secondary cracks, normal to the direction of crack growth, are present.

2. As the crack extends farther from the notch, facets are progressively replaced by dimples, and eventually only dimples can be seen.

3. The arc-shaped beach mark and the crack jump zones of the R = 0.5 specimens and the overload fracture areas of the R = 0.5 and 0.1 specimens are covered with dimples. (No fatigue striation can be seen in the beach mark zones of the R = 0.5 specimens.)

4. Particles of various sizes and shapes are present throughout the areas of slow crack growth, crack jumping, and overload fracture. Some of the particles are clustered closely. (These particles are presumably oxides and Co_2Al_9 or $[Co, Fe]_2Al_9$.)

The SEM fractographs of the I/M 7475-T7351 aluminum alloy specimens, fatigue-tested under constant-amplitude loadings of R = 0.1 and 0.5, show facets in the entire area of slow crack growth (see Figures 25 and 26). Some facets contain river patterns.

The SEM fractographs of the P/M 7091-T7E69 aluminum alloy specimens, fatigue-tested under FALSTAFF and MINI-TWIST spectrum loadings, illustrate the following (see Figures 27 and 28):

1. The beach mark zone adjoining the notch contains facets. Most of them contain river patterns. Secondary cracks run normal to the crack growth direction.

2. In the beach mark zones having a parabolic shape, facets with river patterns can be seen.

3. The crack jump zone between beach mark zones is covered with numerous dimples. Many of the dimples contain small particles, presumably oxides. (This observation indicates nucleation of

micro-voids at oxide particles and resultant crack jumping.)

4. The overload fracture zone is also covered with dimples.

SEM fractographs of the I/M 7475-T7351 aluminum alloy specimens, fatigue-tested under FALSTAFF and MINI-TWIST spectrum loadings, are contained in Figures 29 and 30. They show facets with river patterns in the immediate vicinity of the notch (or the fatigue crack initiation site) and sharply delineated fatigue striations in the remainder of the slow crack growth area. Secondary cracks can be seen along some of the striations.

DISCUSSION

The measured values of tensile yield strength and ultimate tensile strength of the P/M 7091-T7E69 aluminum alloy are superior to those of the I/M 7475-T7351 aluminum alloy, as shown in Tables 2 and 3. However, the elongation and fracture toughness,[6] K_{Ic} or K_Q, of the former are much lower than those of the latter, as shown in Tables 2, 3, and 6. The low ductility and fracture toughness must be closely associated with the inferior fatigue resistance of the P/M 7091-T7E69 aluminum alloy.

The fatigue crack in the I/M 7475-T7351 aluminum alloy specimens is straight and perpendicular to the loading axis, whereas that in the P/M 7091-T7E69 aluminum alloy specimens exhibits a tortuous profile. Metallographic examination of the latter reveals that the fatigue crack growth path is partly along prior powder boundaries (PPB) or grain boundaries (GB) in some areas but it is usually transgranular and deflects frequently at PPB or GB (see Figure 31). Such microstructurally induced deflections of fatigue cracks also were observed in other alloys such as 2020-T651 aluminum,[17] underaged 7075 aluminum,[18] Al-Li base alloys,[19-23] Fe-2Si-0.1C steel,[17,24] AISI 1018 steel,[25] and Ti-6Al-4V alloy.[26] The mechanism of fatigue crack deflection and the mechanics of continued crack growth along the tortuous path are not clearly understood. Some investigators[18-20,27] attribute the crack path tortuosity to intense shear on and cracking along localized crystallographic planes such as the {111} in aluminum alloys and the (0001) and {10T0} in titanium alloys.

In the P/M 7091-T7E69 aluminum alloy specimens, dark zones of crack jumping are seen within the slow crack growth area of the fatigue fracture surface, except for constant-amplitude loading fatigue with R = 0.1. Such a crack jump zone is much larger under the FALSTAFF and MINI-TWIST spectrum loadings than under the constant-amplitude loading with R = 0.5. The crack jump zone is completely covered with dimples, many of which contain small particles, presumably oxides. This indicates that the crack jumping arises from nucleation of microvoids at many oxide particles and their growth and coalescence ahead of an advancing crack tip under fatigue loading. The crack jumping

results in a large increment of crack entension. Such crack jumping and large crack extension in a P/M 7091-T7E69 aluminum alloy die forging were also reported by Wanhill.[28] He attributed the crack jumping to microvoid nucleation at oxide particles on the basis of Thomason's theory[29] for cavity nucleation at second-phase particles and ductile fracture.

CONCLUSIONS

The P/M 7091-T7E69 aluminum alloy has less directon-sensitive tensile properties, greater tensile yield strength, and greater ultimate tensile strength than those of I/M 7475-T7351 aluminum alloy. The fracture toughness of the former, however, is much lower than that of the latter. Microstructures of P/M 7091-T7E69 and I/M 7475-T7351 aluminum alloys differ because of extra phases in P/M 7091-T7E69 aluminum alloy: Co_2Al_9 or $[Co,Fe]_2Al_9$ and oxides. The Co_2Al_9 or $[Co,Fe]_2Al_9$ appear as spheroids and is not deformed or fractured by the forging process. The oxides appear as numerous particles of irregular shapes and are smaller than the Co_2Al_9 or $[Co,Fe]_2Al_9$ particles. Both kinds of particles are present along the prior particle boundaries (PPB) and grain boundaries (GB) as well as within the powder.

The fatigue crack growth path is tortuous and deviates from the symmetry plane in P/M 7091-T7E69 aluminum alloy, whereas the crack growth path is regular and normal to the loading axis in I/M 7475-T7351 aluminum alloy. The crack tortuosity in P/M 7091-T7E69 aluminum alloy arises from frequent crack deflection and occasional crack growth at and along PPB or GB. Crack jumping occurs in P/M 7091-T7E69 aluminum alloy under fatigue loading except for constant-amplitude loading with R = 0.1. Crack jumping is quite extensive under the FALSTAFF and MINI-TWIST spectrum loadings and shortens the fatigue crack growth lives drastically. It is induced by nucleation of microvoids at the numerous oxide particles and their growth and coalescence ahead of an advancing crack tip.

REFERENCES

1. Froes, F.H. and Pickens, J.R., "Powder Metallurgy of Light Metal Alloys for Demanding Applications," Journal of Metals, Vol. 36, No.1 Jan 1984, pp. 14-28.

2. Wanhill, R.J.H. and Schra, L., "Engineering Property Comparisons of PM and IM Aluminum Alloy Forgings," NLR MP 83066 U, National Aerospace Laboratory, The Netherlands, Nov 1983.

3. Petrak, G.J. and Malas, M.A., "The Mechanical Property Data Base from a Cooperative Program on First Generation PM Aluminums," AFWAL-TR-85-4052, Air Force Wright Aeronautical Laboratories, Wright-Patterson Air Force Base, OH, Aug 1985.

4. Ruschau, J.J., "Mechanical Property Data on P/M Aluminum X7091-T7E69 Extrusion," AFWAL-TR-82-4161, University of Dayton Research Institute, Dayton, OH, Oct 1982.

5. Santner, J.S. and Kumar, M., "Corrosion-Fatigue Crack Propagation Rates in Commercial 7075 and P/M X7091 Aluminum Alloys" in "Corrosion Fatigue: Mechanics, Metallurgy, Electrochemistry, and Engineering," ASTM STP 801, T.W. Crooker and B.N. Leis, Eds., American Society for Testing and Materials, 1983, pp. 229-255.

6. Schra, L. and 'tHart, W.G.J., "Engineering Property Comparisons of PM Alloy X7091-T7E69 and IM Alloy Forgings, "NLR TR 82054 U, National Aerospace Laboratory, The Netherlands, Jun 1982.

7. Rafalin, M., "Fatigue of High Strength Powder Metallurgy Aluminum Alloys," PhD Thesis, Drexel University, Philadelphia, Pa., Jan 1981.

8. Hart, R.M. "Wrought P/M Aluminum Alloys X7090 and X7091," Alcoa Green Letter, Alcoa, Aug 1981.

9. Ruschau, J.J. "Spectrum Fatigue Crack Growth Rate Characteristics of PM Aluminums 7090 and 7091," AFWAL-TR-83-4032, University of Dayton Research Institute, Dayton, OH, Apr 1983.

10. Bretz, P., "Spectrum Fatigue Behavior, An Update," Wrought P/M Alloys Tech Brief, Alcoa, Mar 1984.

11. van Dijk, G.M. and de Jonge, J.B., "Introduction to a Fighter Aircraft Loading Standard for Fatigue Evaluation FALSTAFF", Paper 3.61, Eighth ICAF Symposium, Lausanne, 1975.

12. de Jonge, J.B., Schütz, D., Lowak, H., and Schijve, J.,"A Standardized Load Sequence for Flight Simulation Tests on Transport Aircraft Wing Structures," LBF-Bericht FB-106, NLR TR 73029 U, Mar 1973.

13. Lowak, H., de Jonge, J.B., Franz, J., and Schütz, D., "MINI-TWIST a Shortened Version of TWIST," LBF-Report No. FB-146, 1979, NLR MP 79018 U, May 1979.

14. ASTM Standard E647-83, "Standard Test Method for Constant-Load-Amplitude Fatigue Crack Growth Rates above 10^{-8}m/cycle," 1985 Annual Book of ASTM Standards, Vol. 03.01, pp. 739-755.

15. Kim, Y.W., Griffith, W.M., and Froes, F.M., "The Breakup and Distribution of Surface Oxides Through Processing of P/M Aluminum Alloy 7091," Presented at 1983 ASM Metals Congress, Philadelphia, Pa., 3-6 Oct 1983, Metals/Materials Technology Series 8305-048, ASM, Metals Park, Ohio.

16. Margolis, W.S., "F-16 Material Test Allowables for Aluminum Alloy 7475, 3.0" Plate-T7351 Temper, and 0.5" Plate (92" Width)-T7651 Temper and -T7351 Temper," Report No. 16PR926, Apr 1978, General Dynamics, Fort Worth, Tex.

17. Suresh, S., "Crack Deflection: Implications for the Growth of Long and Short Fatigue Cracks," Met Trans A, Vol. 14A; Nov 1983, pp. 2375-2385.

18. Suresh, S., Vasude'van, A.K., and Bretz, P.E., "Mechanisms of Slow Fatigue Crack Growth in High Strength Aluminum Alloys: Role of Microstructure and Environment," Met Trans A, Vol. 15A, Feb 1984, pp. 369-379.

19. Vasude'van, A.K., and Suresh, S., "Lithium-Contalning Aluminum Alloys: Cyclic Fracture," Met Trans A., Vol. 16A, Mar 1985, pp. 475-477.

20. Harris, S.J., Noble, B., and Dinsdale, K., "Fatigue Crack Growth Characteristics of Al-Li Based Alloys," in "Fatigue 84, Vol. 1", ed. C.J. Beevers, Engineering Material Advisory Services Ltd., West Midlands, U.K., 1984, pp. 361-371.

21. Dinsdale, K., Harris, S.J., and Noble, B., "Relationship between Microstructure and Mechanical Properties of Aluminum-Lithium-Magnesium Alloys," in "Aluminum-Lithium Alloys," ed. T.H. Sanders, Jr. and E.A. Starke, Jr., The Metallurgical Society of AIME, Warrendale, Pa., 1981, pp. 101-118.

22. Harris, S.J., Noble, B., and Dinsdale, K., "Effect of Composition and Heat Treatment on Strength and Fracture Characteristics of Al-Li-Mg Alloys," in "Aluminum-Lithium Alloys II," ed. E.A. Starke, Jr. and T.H. Sanders, Jr., The Metallurgical Society of AIME, Warrendale, Pa, 1984, pp. 219-233.

23. Ruch, W., Jata, K., and Starke, E.A., Jr. "The Fatigue Crack Propagation Behavior of New Al-Li-X Alloys," in "Fatigue 84, Vol. 1," ed. C.J. Beevers, Engineering Materials Advisory Services Ltd., West Midlands, U.K., 1984, pp. 145-161.

24. Dutta, V.B., Suresh, S., and Ritchie, R.O., "Fatigue Crack Propagation in Dual-Phase Steels: Effects of Ferritic-Martensitic Microstructures on Crack Path Morphology," Met Trans A, Vol. 15A, June 1984, pp. 1193-1207.

25. Suzuki, H., and McEvily, A.J., "Microstructural Effects on Fatigue Crack Growth in a Low Carbon Steel," Met Trans A, Vol. 10A, Apr 1979, pp. 475-481.

26. Bania, P.J., and Eylon, D., "Fatigue Crack Propagation of Titanium Alloys Under Dwell-Time Conditions," Met Trans A, Vol. 9A, June 1978, pp. 847-855.

27. Suresh, S., "Fatigue Crack Deflection and Fracture Surface Contact: Micromechanical Models," Met Trans A, Vol. 16A, Feb 1985, pp. 249-260.

28. Wanhill, R.J.H., "Fatigue and Fracture Resistance of Wrought PM 7091 and IM 7050," National Aerospace Laboratory NLR, Emmeloord, The Netherlands.

29. Thomason, P.F, "A Theoretical Relation Between K_{IC} and Basic Material Properties in Ductile Metals," International Journal of Fracture Mechanics, Vol. 7, No. 4, Dec 1971, pp 409-419.

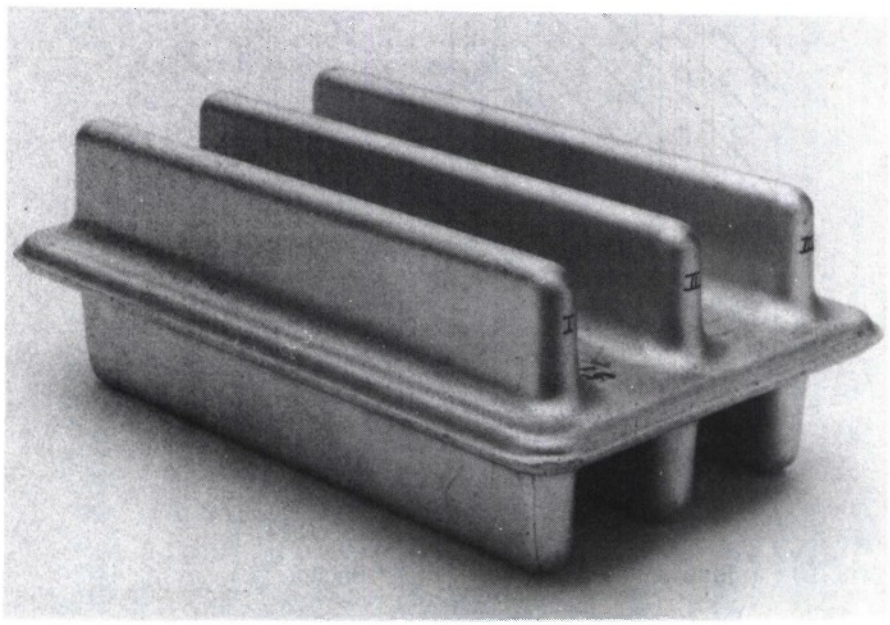

Figure 1. Die Forging of P/M 7091-T7E69 Aluminum Alloy.

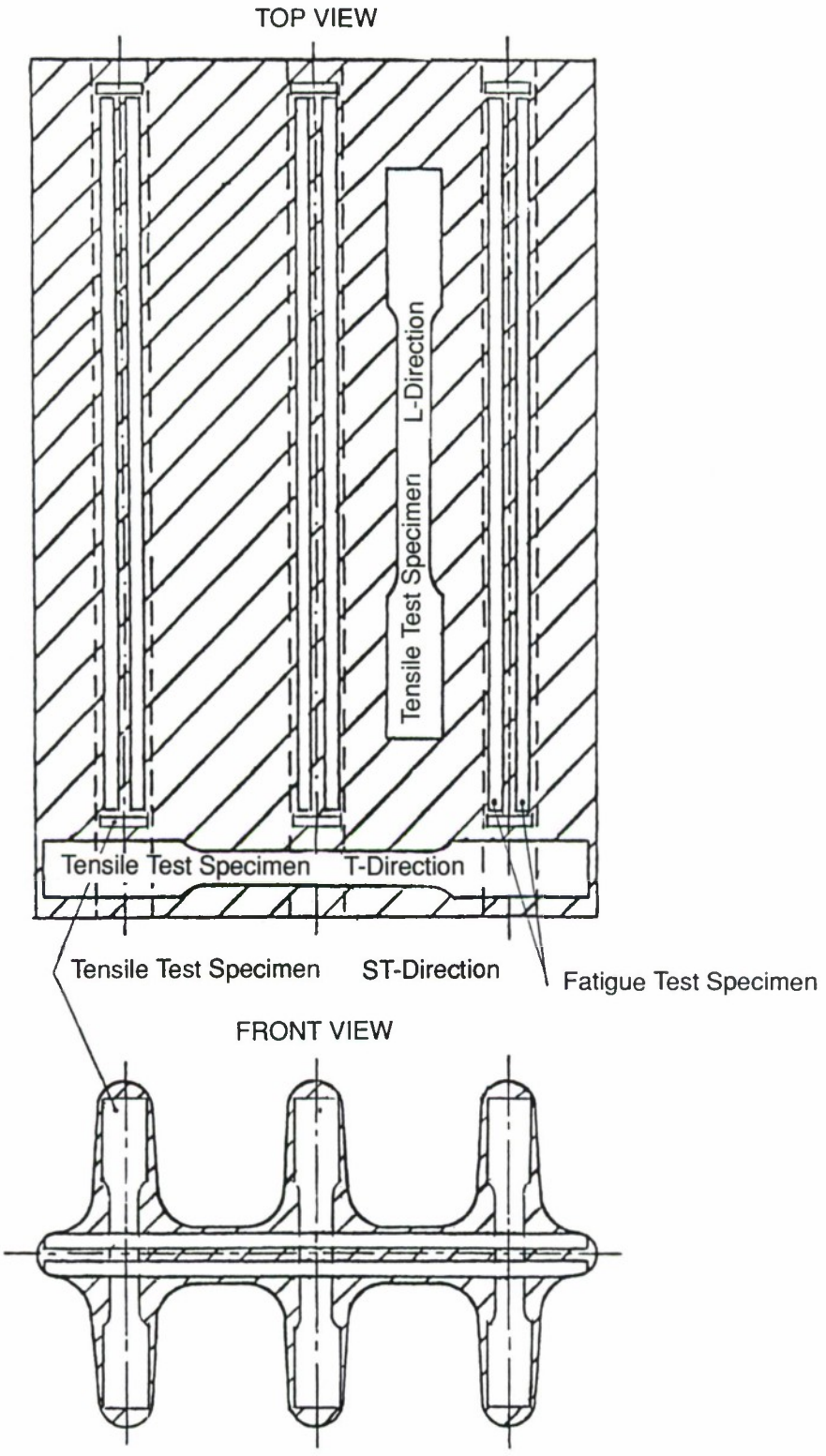

Figure 2. Specimen Positions in Die Forging of P/M 7091-T7E69 Aluminum Alloy.

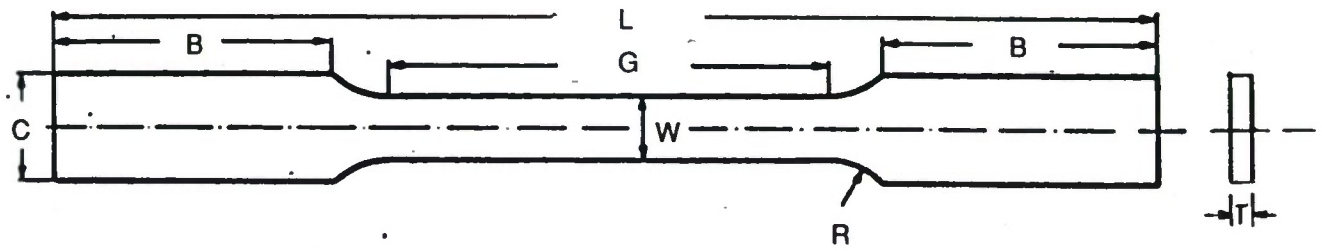

Dimensions (mm)

	L-Direction	T-Direction	ST-Direction
G	50	50	25
W	12.5	12.5	12.5
T	6	6	5
R	13	13	13
L	200	196	120
B	50	48	30
C	20	20	20

Figure 3. Tensile Test Specimen.

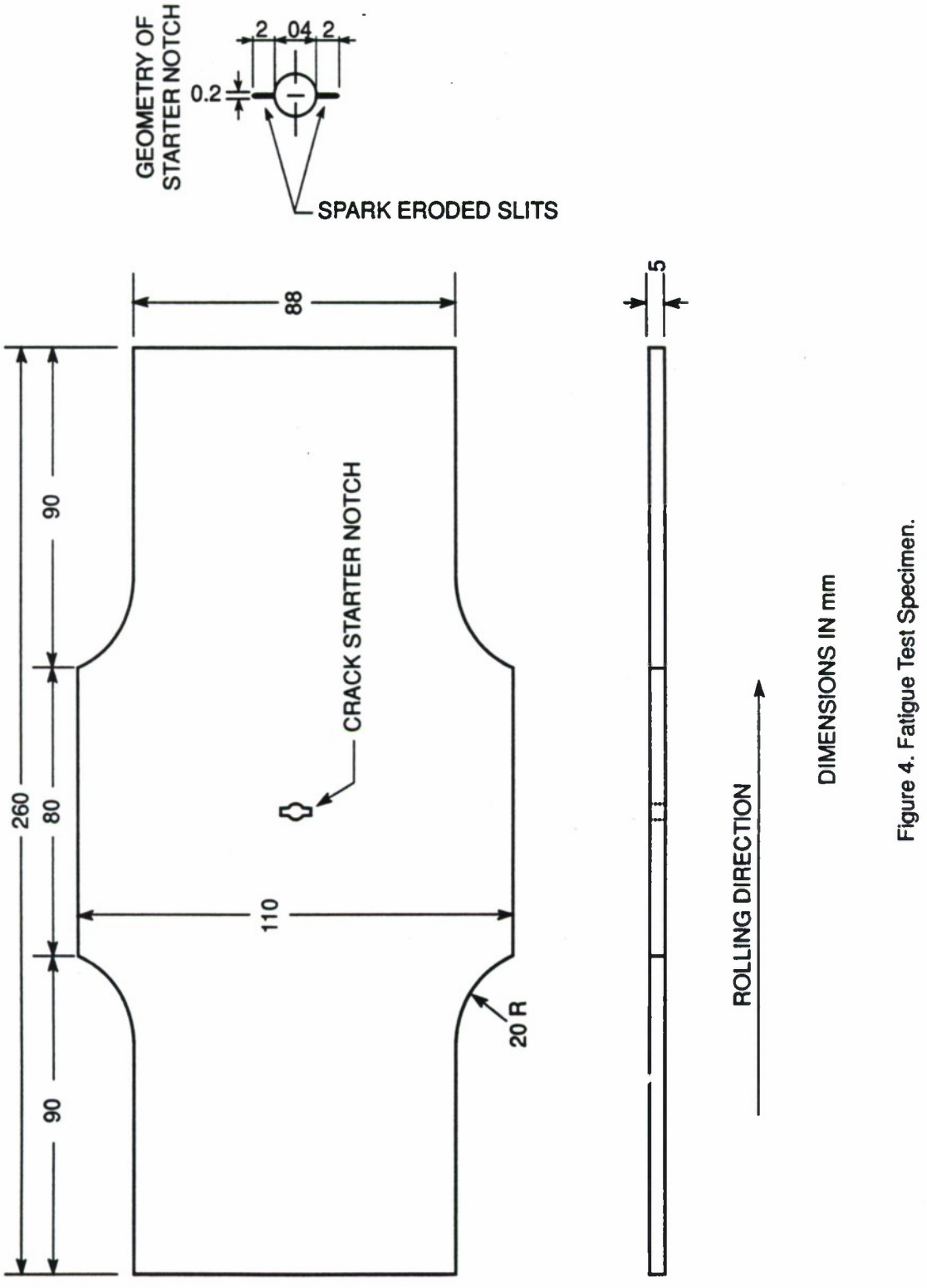

Figure 4. Fatigue Test Specimen.

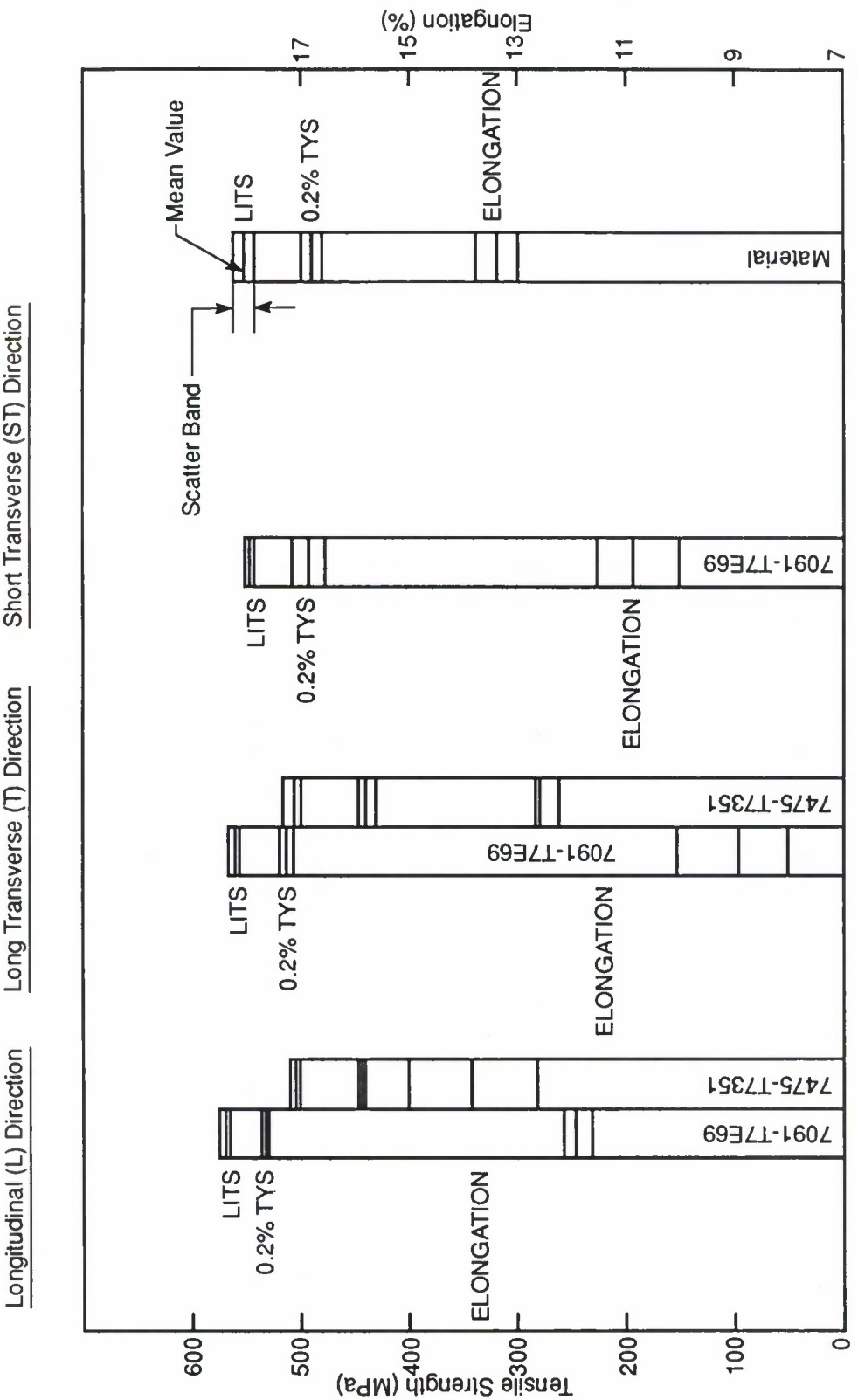

Figure 5. Tensile Properties of P/M 7091-T7E69 and I/M 7475-T7351 Aluminum Alloys.

Figure 6. Fatigue Crack Growth Path in I/M 7475-T7351 Aluminum Alloy, (a), and P/M 7091-T7E69 Aluminum Alloy, (b), under Constant Amplitude Loading.

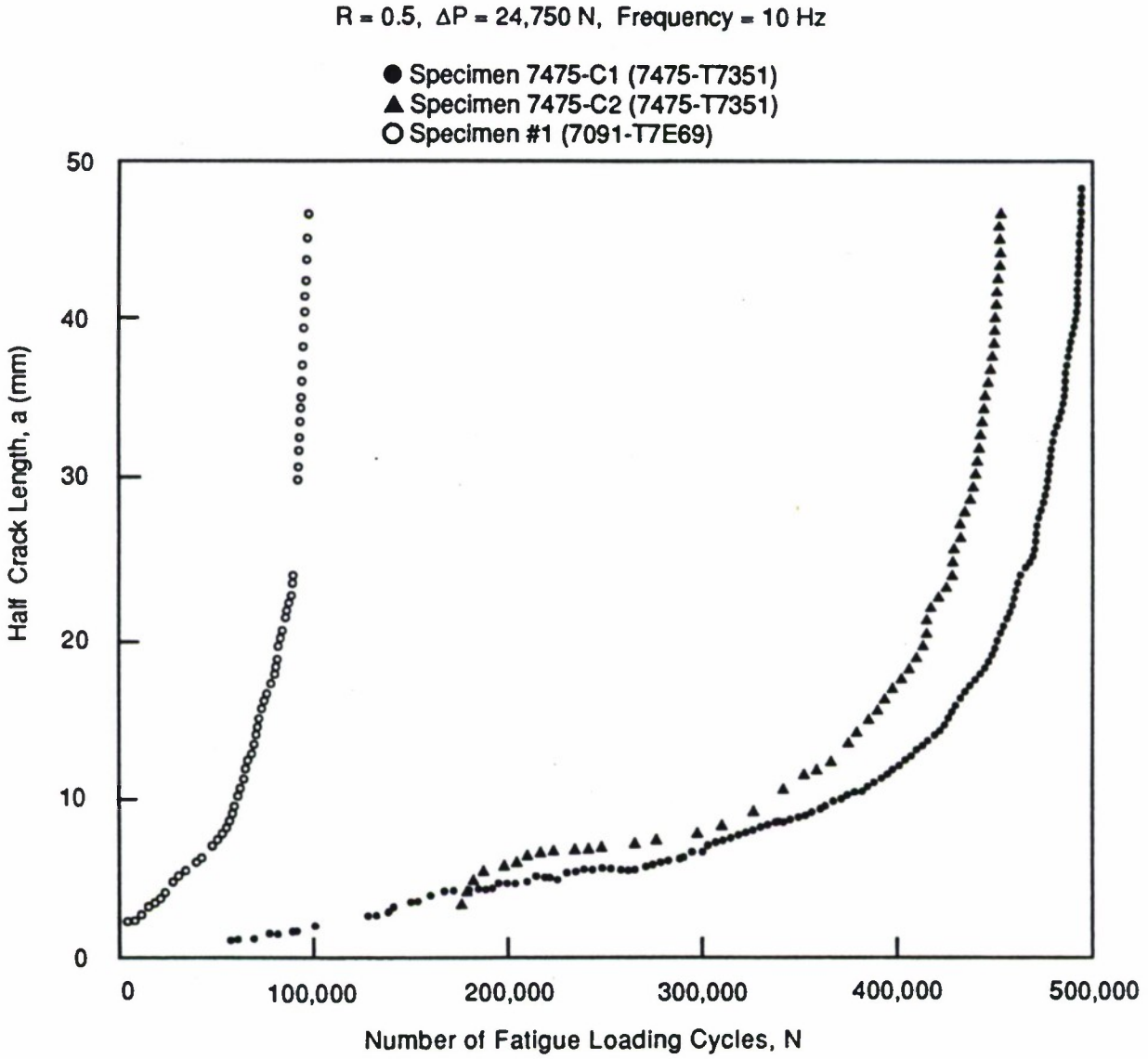

Figure 7. Variation of Half Crack Length, a , with Number of Fatigue Loading Cycles under Constant-Amplitude Loading of R = 0.1.

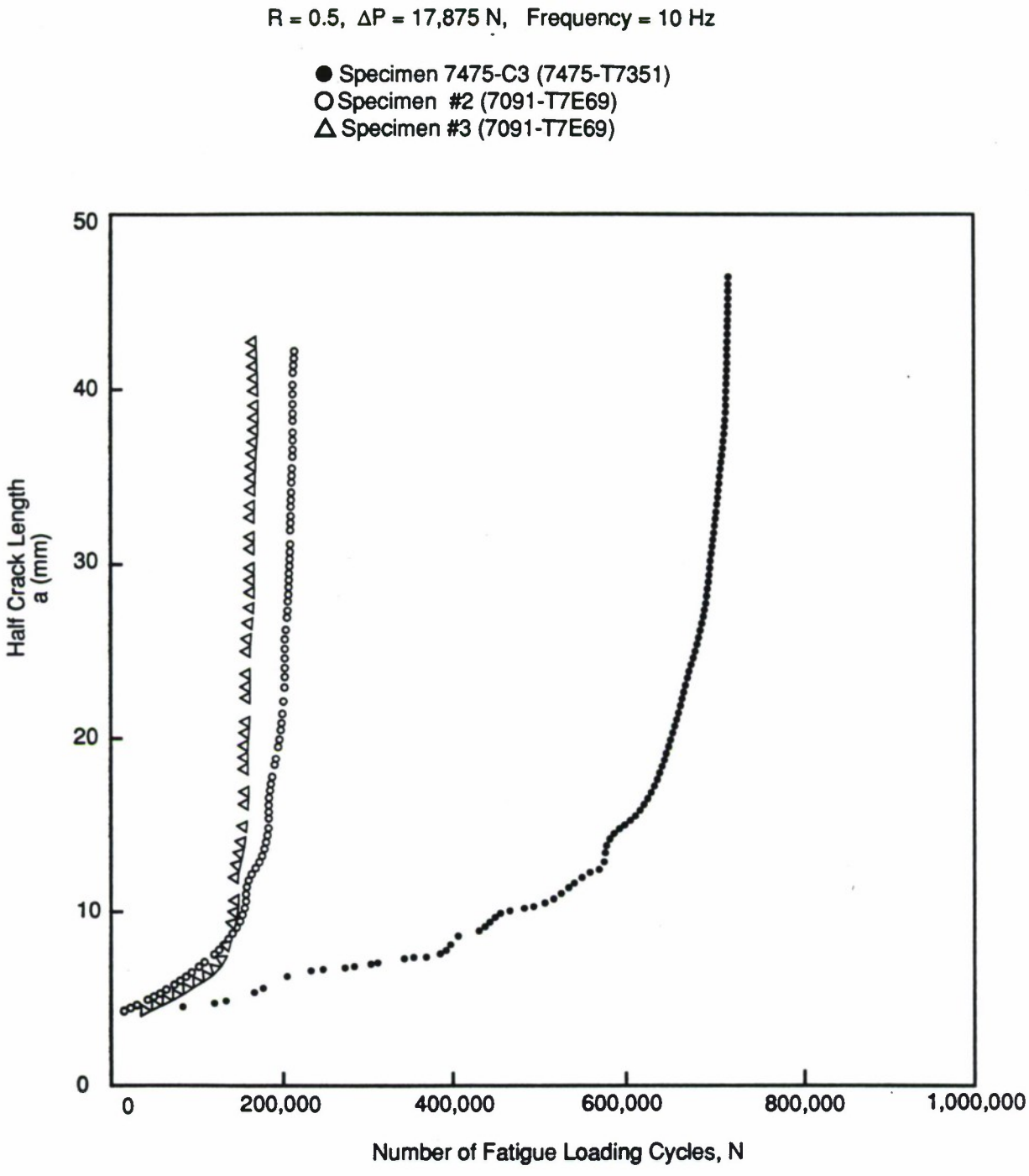

Figure 8. Variation of Half Crack Length, a, with Number of Fatigue Loading Cycles under Constant Amplitude Loading of R = 0.5.

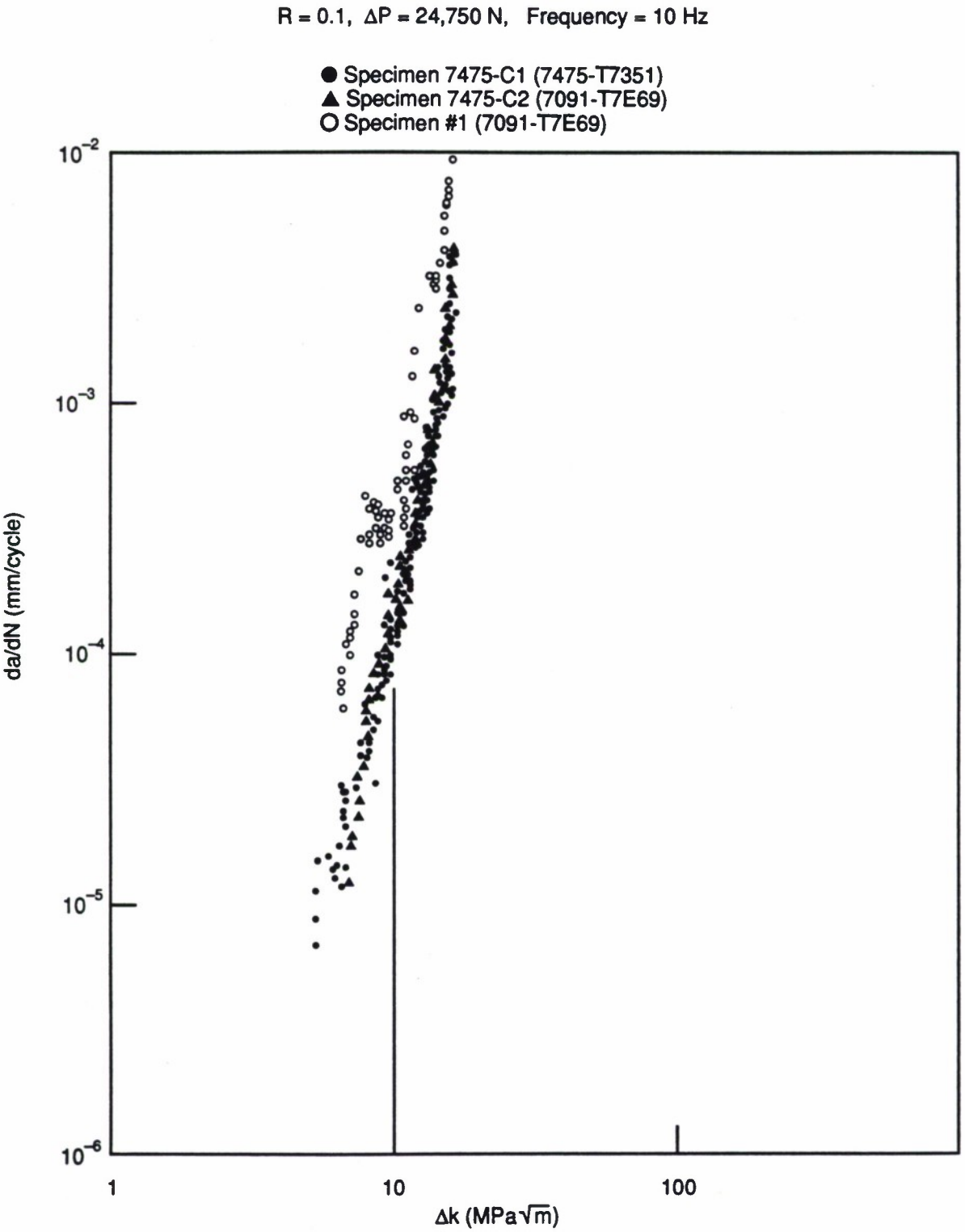

Figure 9. Variations of Fatigue Crack Growth Rate, da/dN, with Stress Intensity Factor Range, Δk, under Constant-Amplitude Loading of R = 0.1.

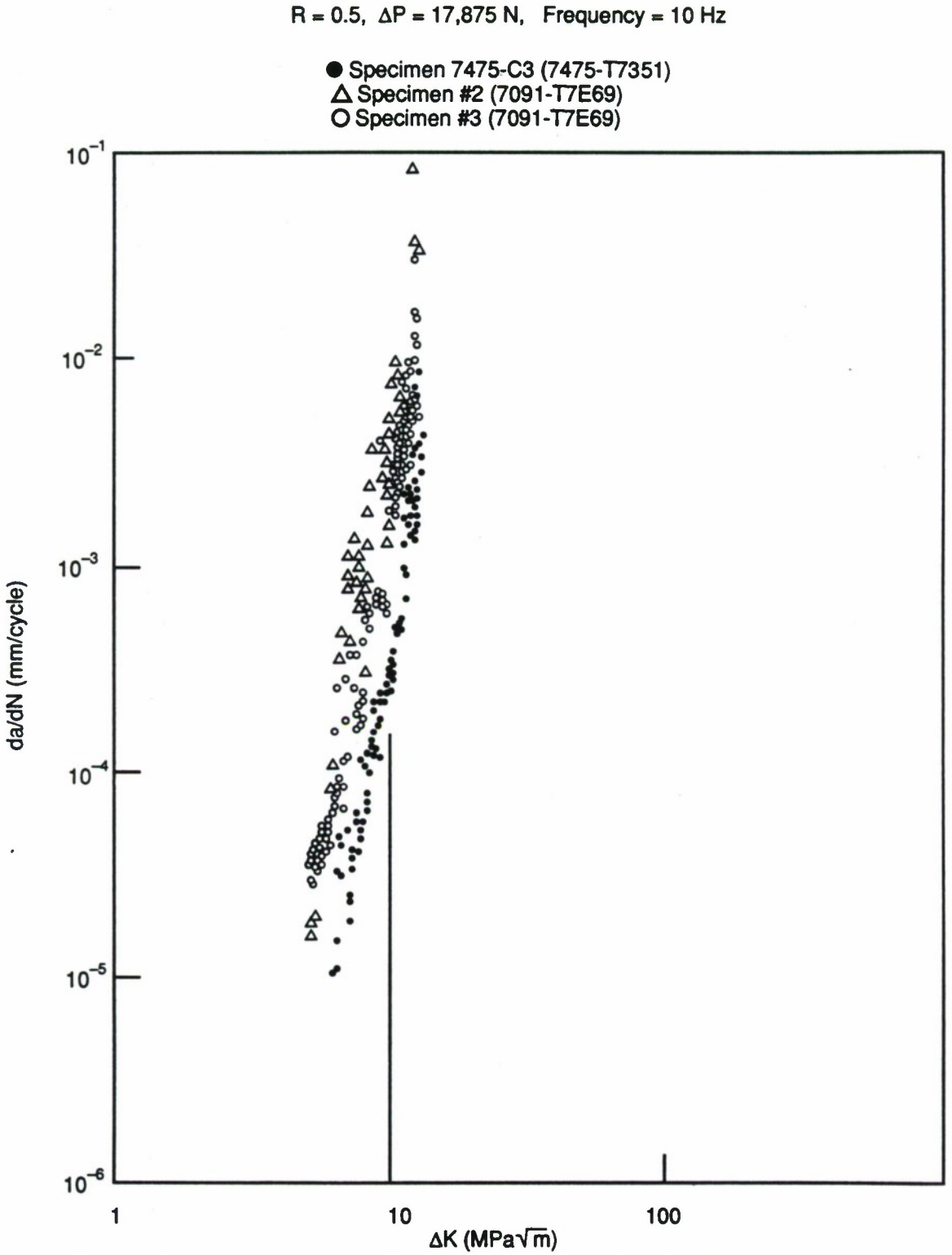

Figure 10. Variation of Fatigue Crack Growth Rate, da/dN, with Stress Intensity Factor Range, ΔK, under Constant-Amplitude Loading of R = 0.5.

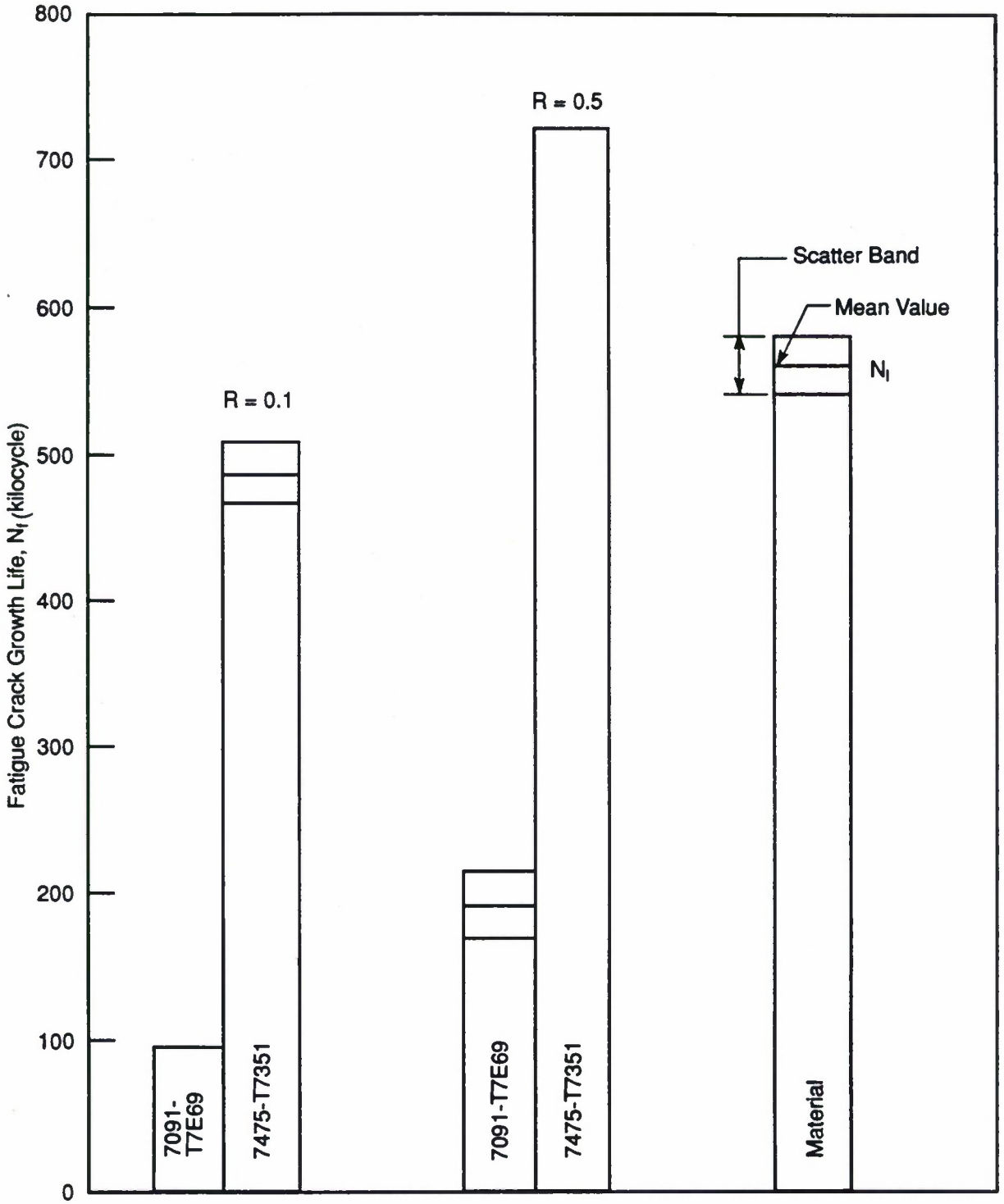

Figure 11. Fatigue Crack Growth Life under Constant-Amplitude Loading.

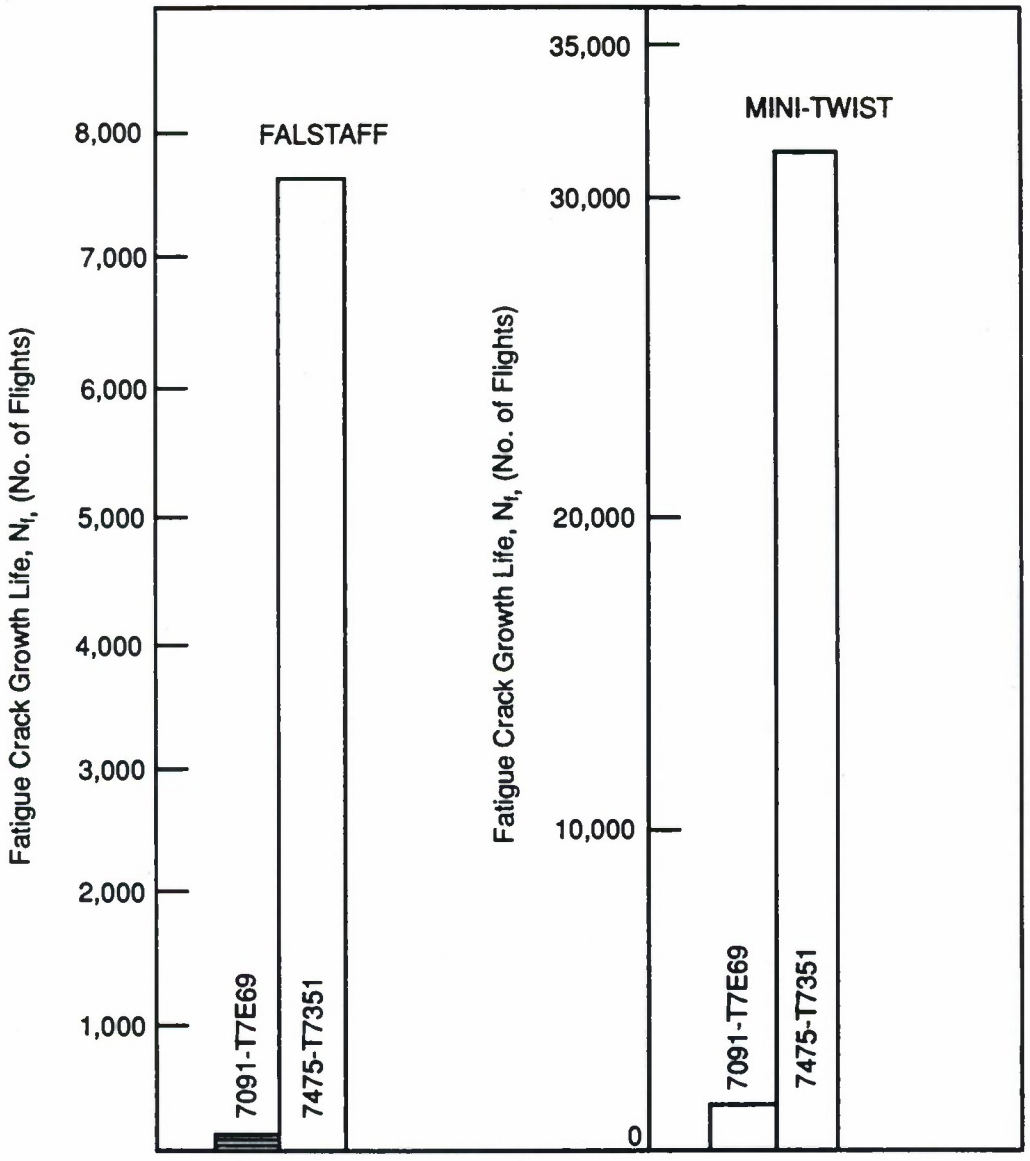

Figure 12. Fatigue Crack Growth Life under Aircraft Spectrum Loading.

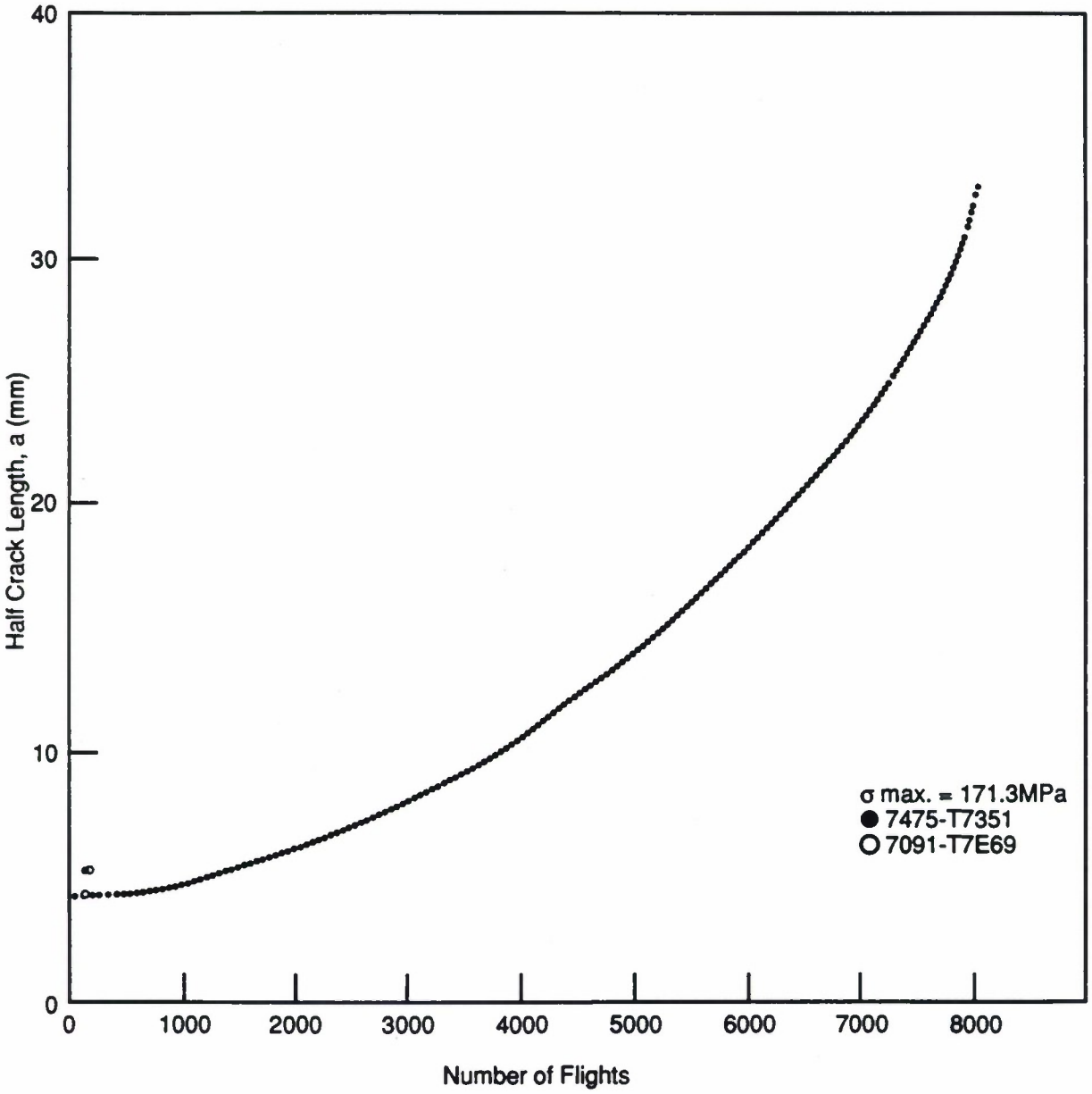

Figure 13. Variation of Half Crack Length, a, with Number of Flights under FALSTAFF Spectrum Loading.

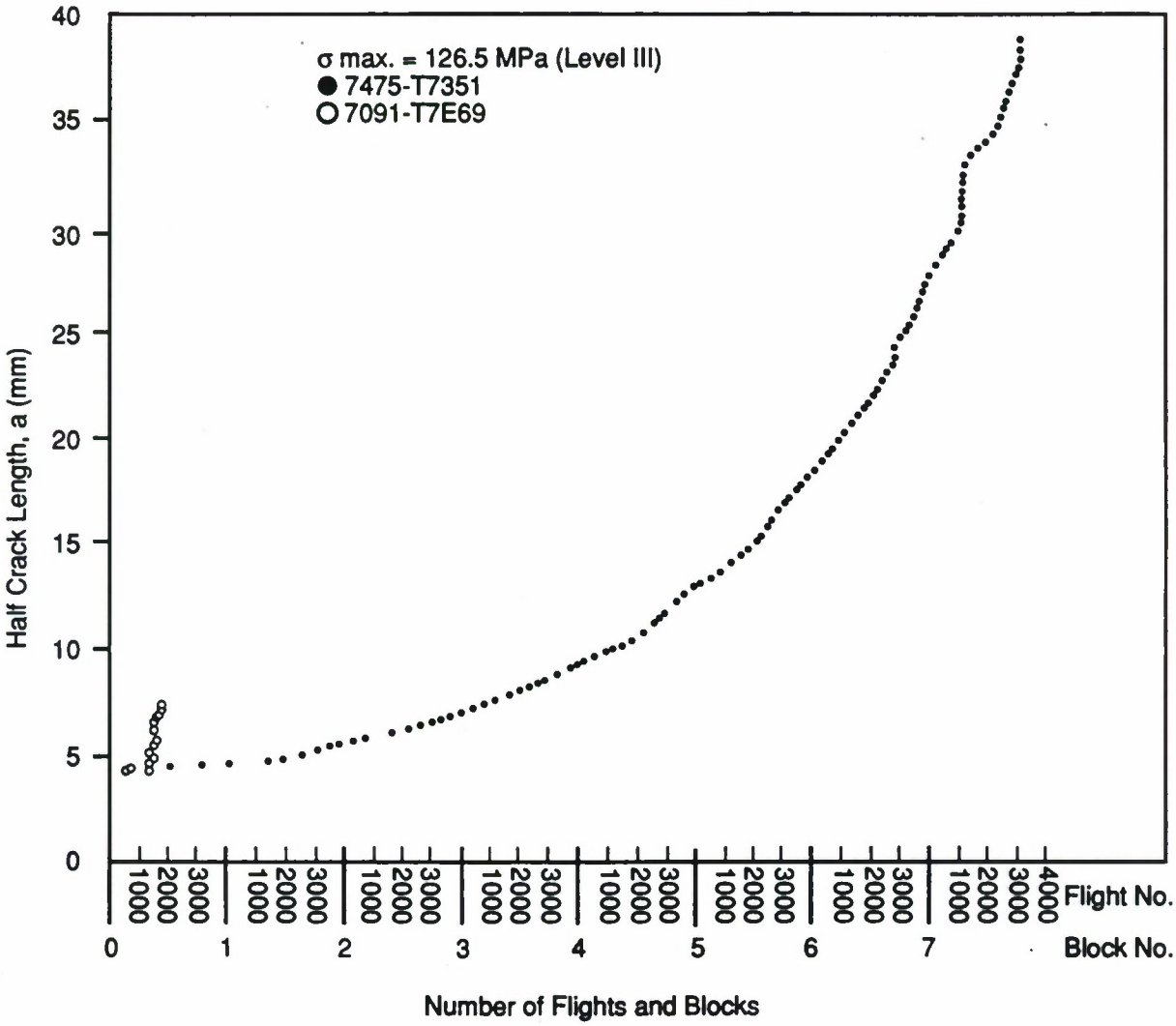

Figure 14. Variation of Half Crack Length, a, with Number of Flights and Blocks under MINI-TWIST Spectrum Loading

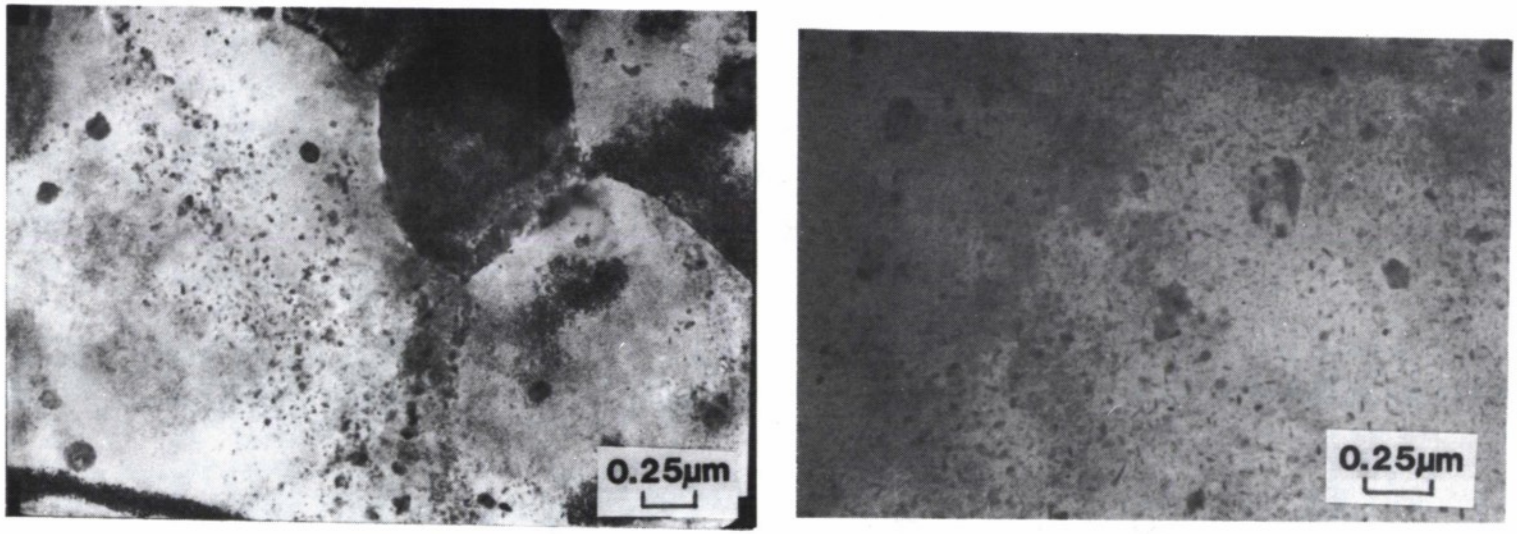

(a) P/M 7091-T7E69 Aluminum Alloy

(b) I/M 7475-T7351 Aluminum Alloy

Figure 15. TEM Micrographs of P/M 7091-T7E69 and I/M 7475-T7351 Aluminum Alloys.

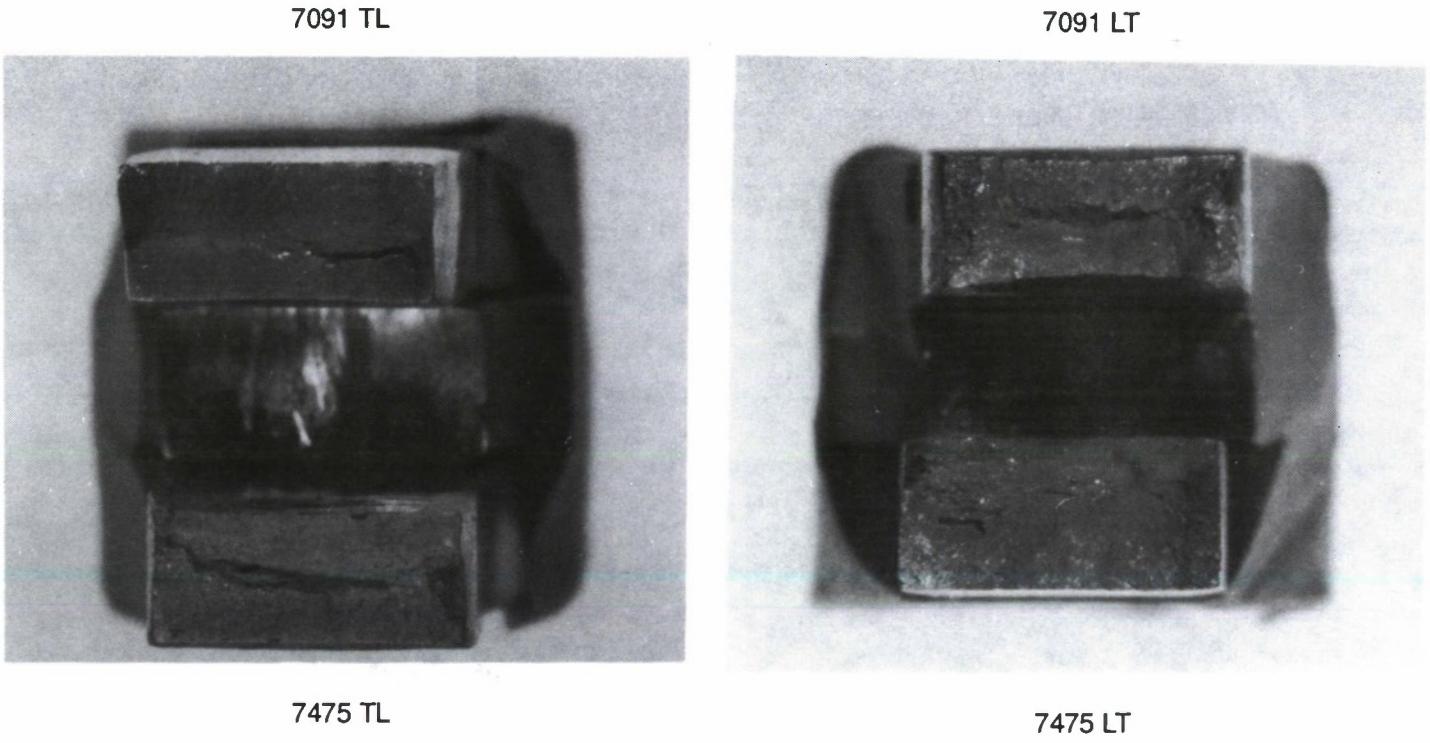

Figure 16. Representative Fracture Surfaces of Tensile Test Specimens (Specimen Orientations LT and TL).

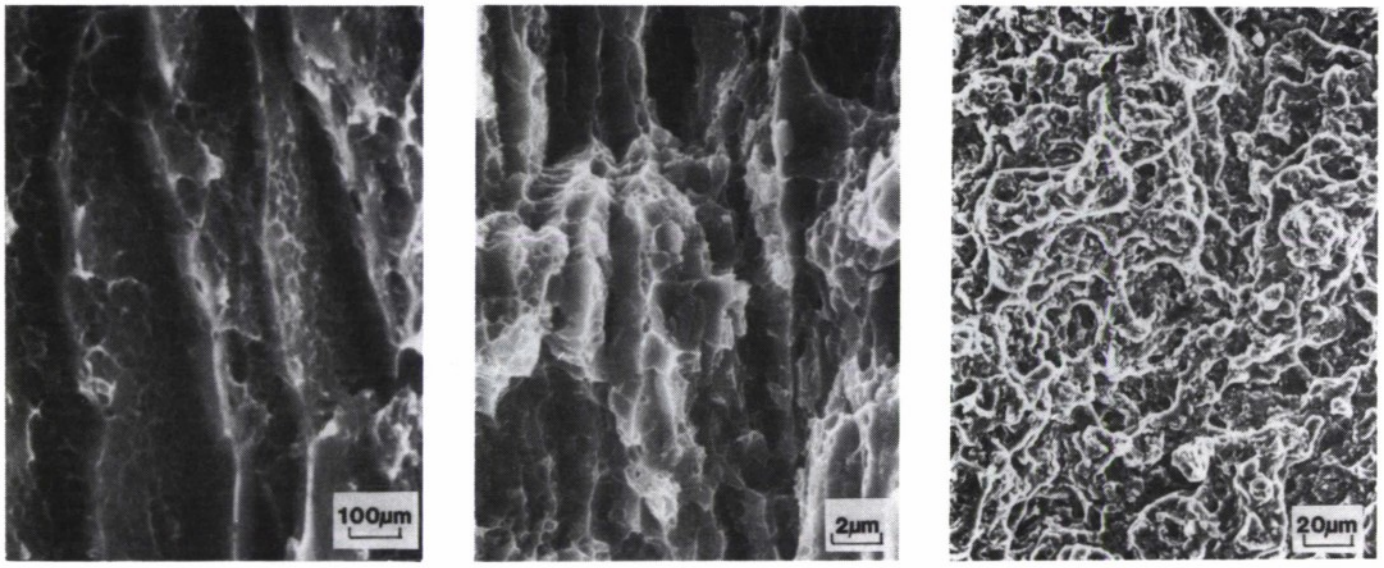

(a) LT-Direction (b) TL-Orientation (c) ST-Orientation

Figure 17. Fractographs of Tensile Test Specimens of P/M 7091-T7E69 Aluminum Alloy.

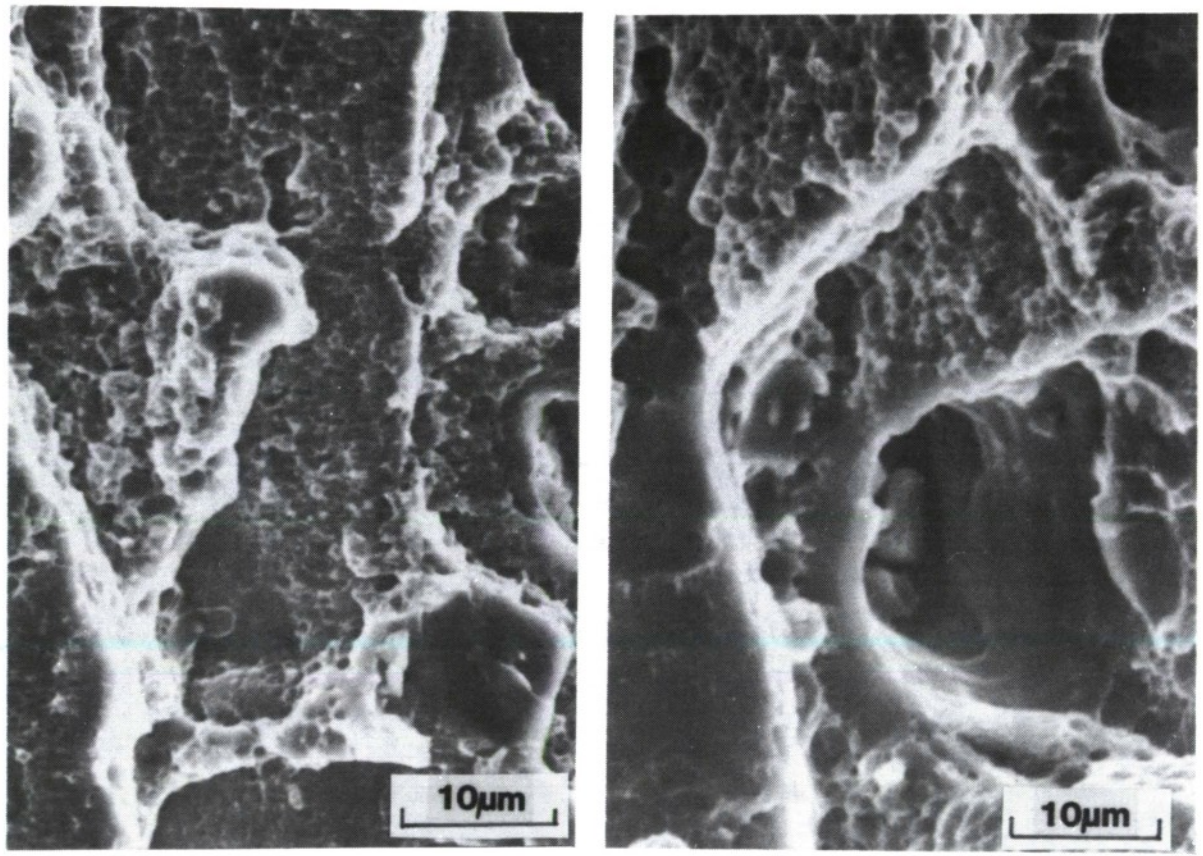

(a) LT-Orientation

(b) TL-Orientation

Figure 18. Fractographs of Tensile Test Specimens of I/M 7475-T7351 Aluminum Alloy.

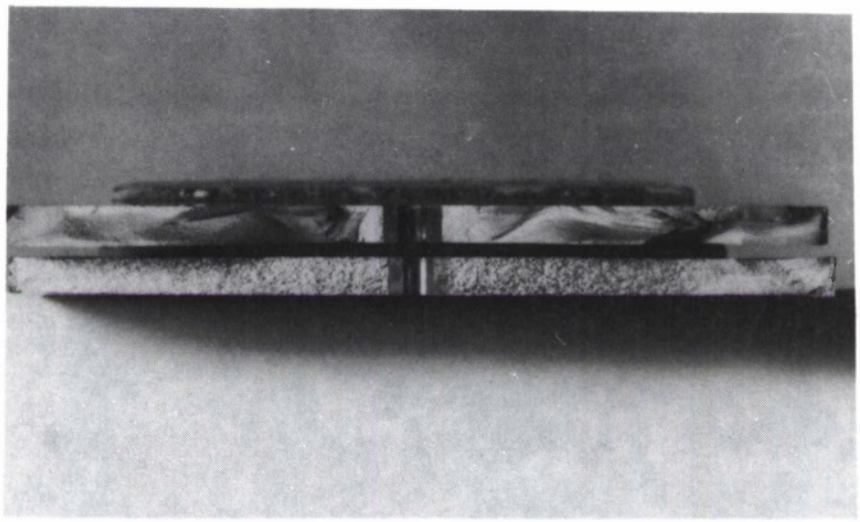

Figure 19. Representative Fracture Surfaces for Constant-Amplitude Loading Fatigue with R=0.1 (Specimen Orientation LS).

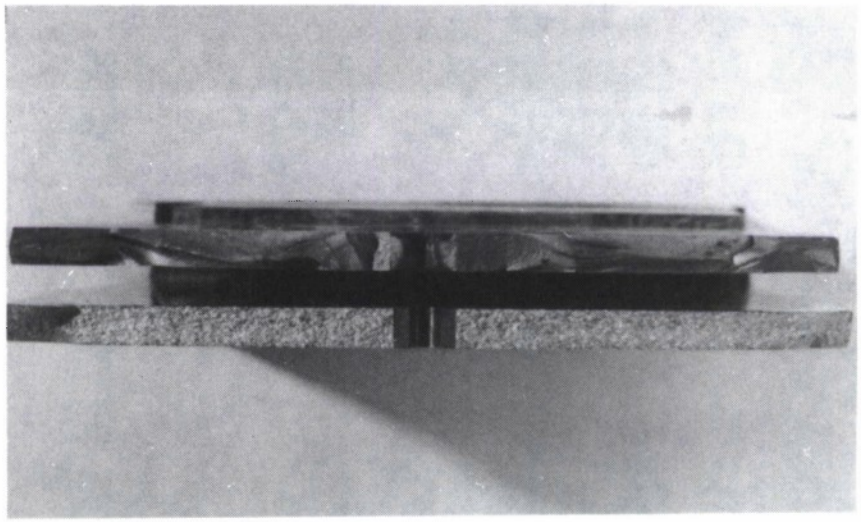

Figure 20. Representative Fracture Surface for Constant-Amplitude Loading Fatigue with R=0.5 (Specimen Orientation LS).

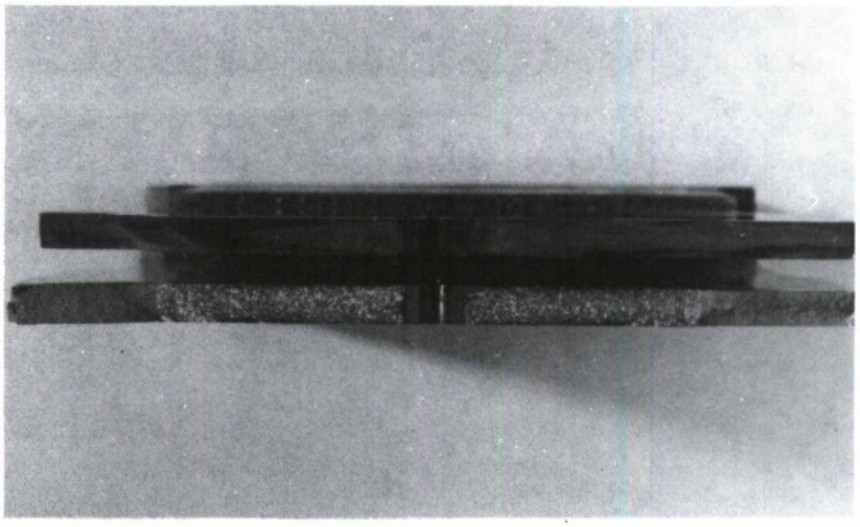

Figure 21. Representative Fracture Surfaces for FALSTAFF Spectrum Loading Fatigue (Specimen Orientation LS).

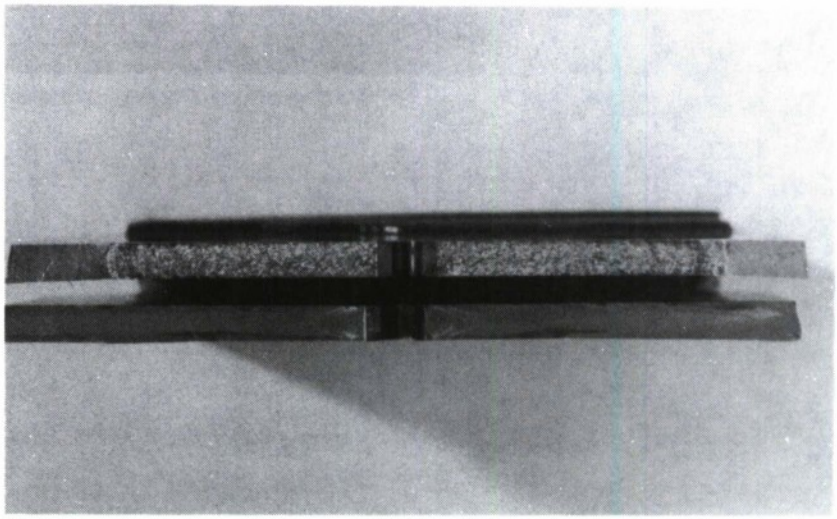

Figure 22. Representative Fracture Surface for MINI-TWIST Spectrum Loading Fatigue (Specimen Orientation LS).

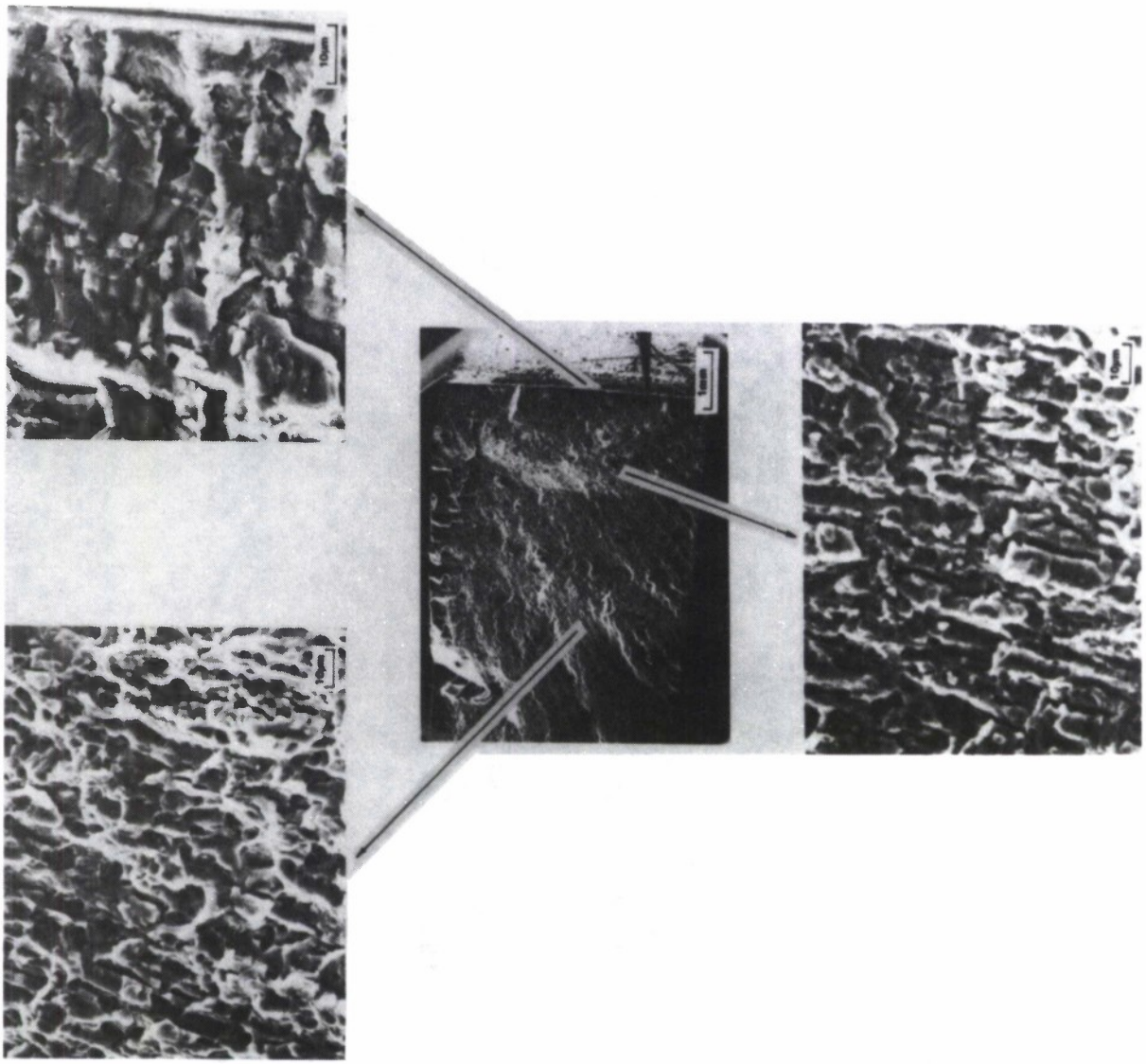

Figure 23. SEM Fractographs of P/M 7091-T7E69 Aluminum Alloy, Fatigue-Tested under Constant-Amplitude Loading with R=0.1.

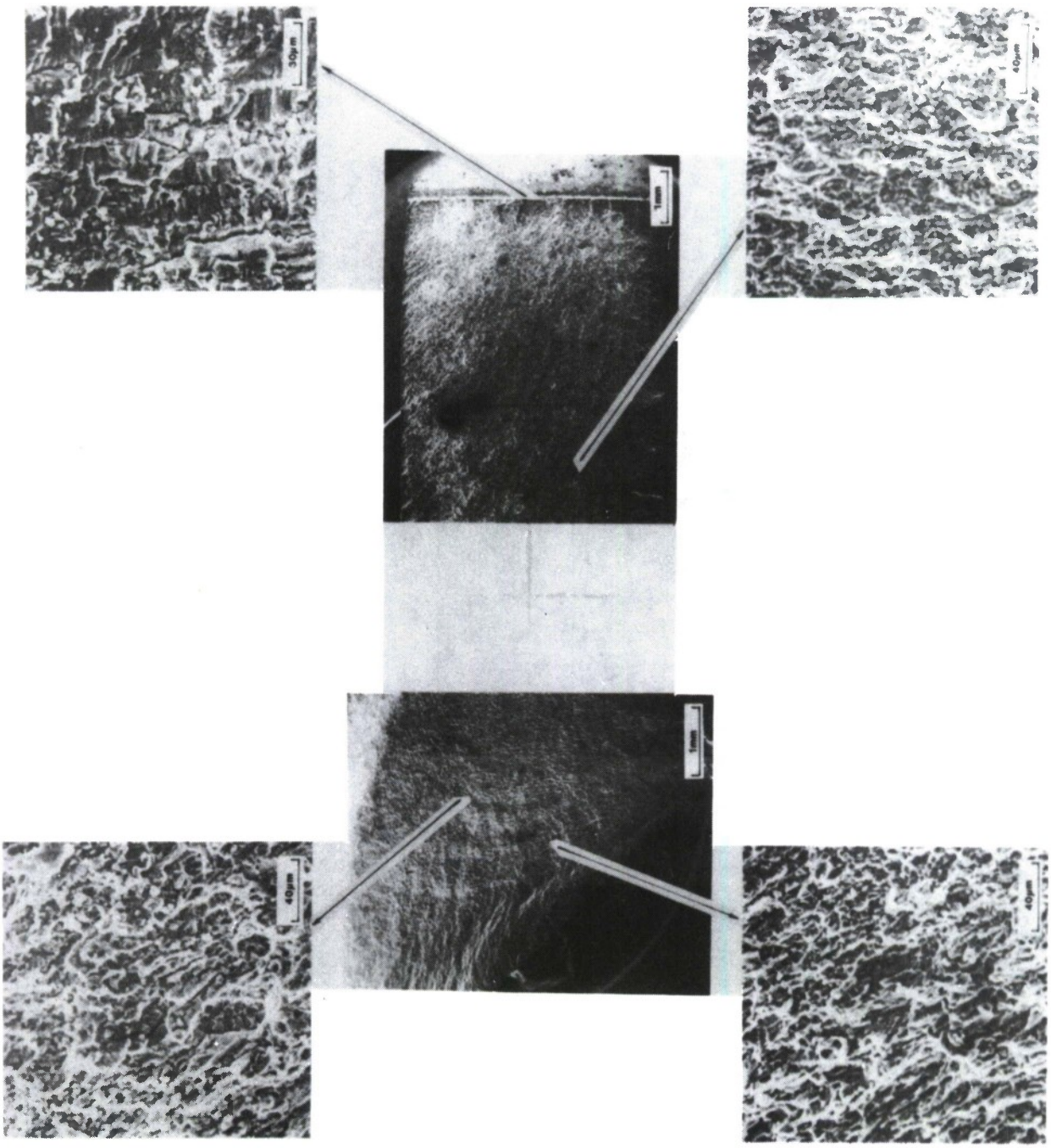

Figure 24. SEM Fractographs of P/M 7091-T7E69 Aluminum Alloy, Fatigue-Tested under Constant-Amplitude Loading with R=0.5.

Figure 25. SEM Fractographs of I/M 7475-T7351 Aluminum Alloy, Fatigue-Tested under Constant-Amplitude Loading with R=0.1.

Figure 26. SEM Fractographs of I/M 7475-T7351 Aluminum Alloy, Fatigue-Tested under Constant-Amplitude Loading with R=0.5.

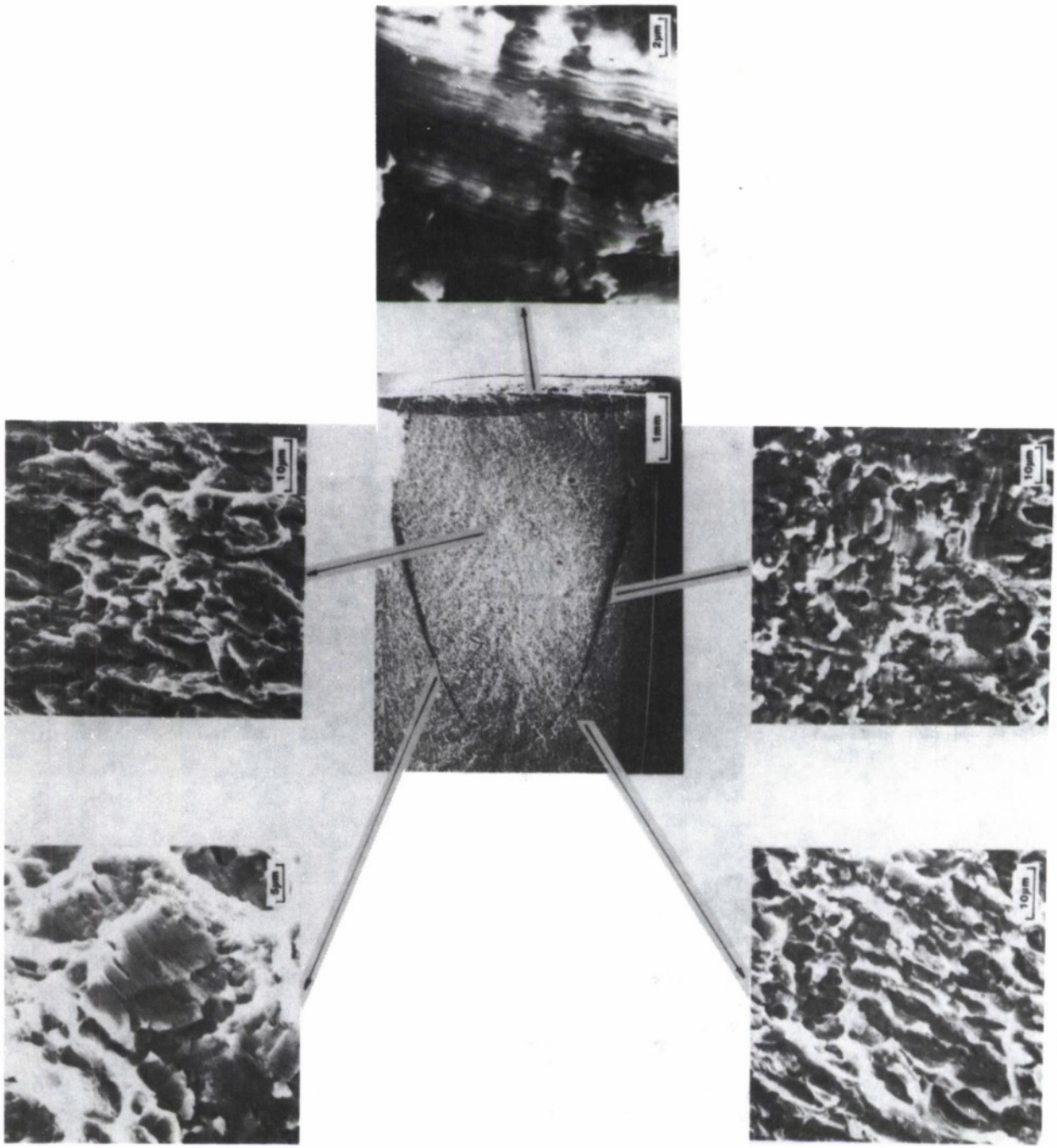

Figure 27. SEM Fractographs of P/M 7091-T7E69 Aluminum Alloy, Fatigue-Tested under FALSTAFF Spectrum Loading.

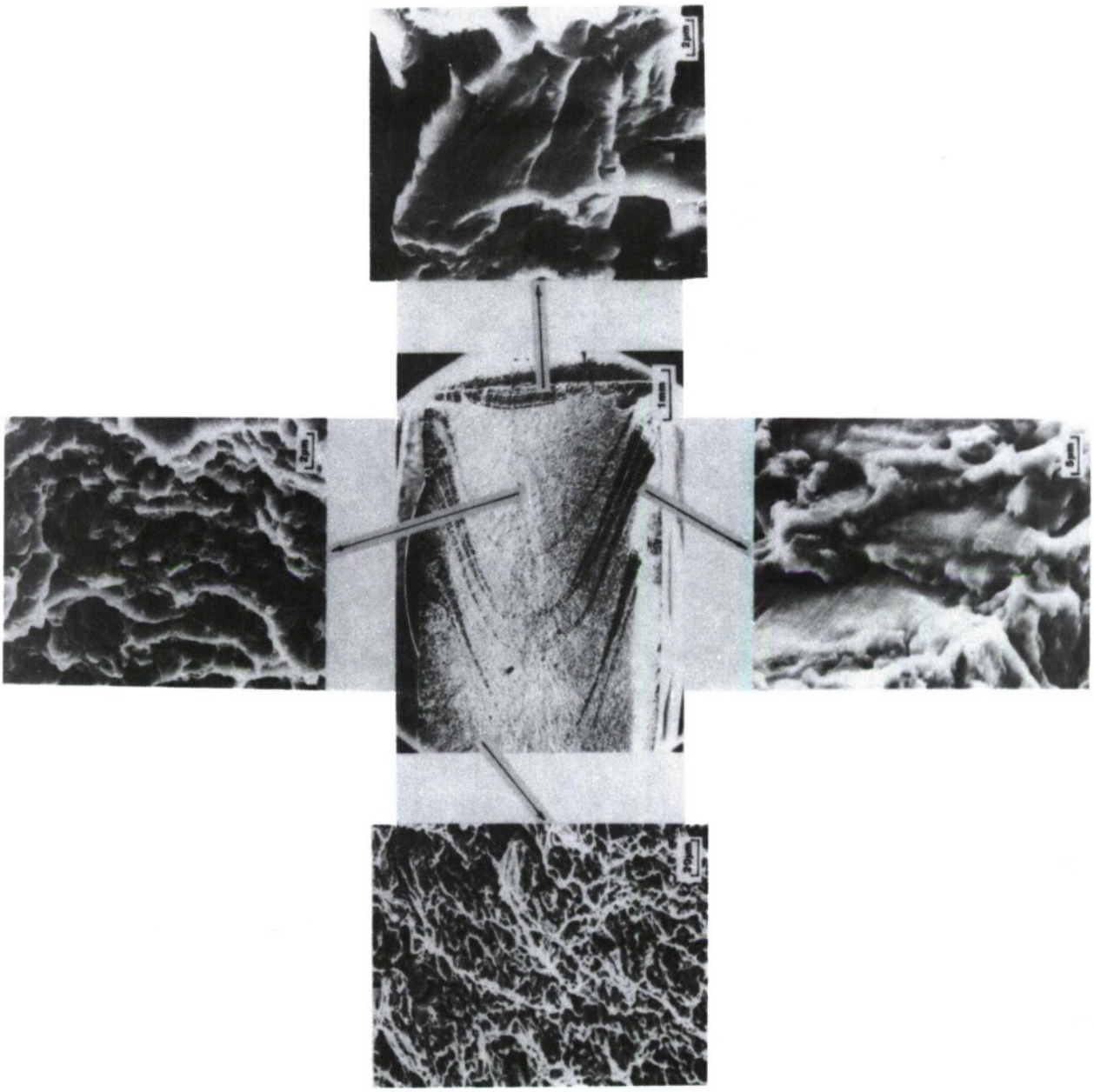

Figure 28. SEM Fractographs of P/M 7091-T7E69 Aluminum Alloy, Fatigue-Tested under MINI-TWIST Spectrum Loading.

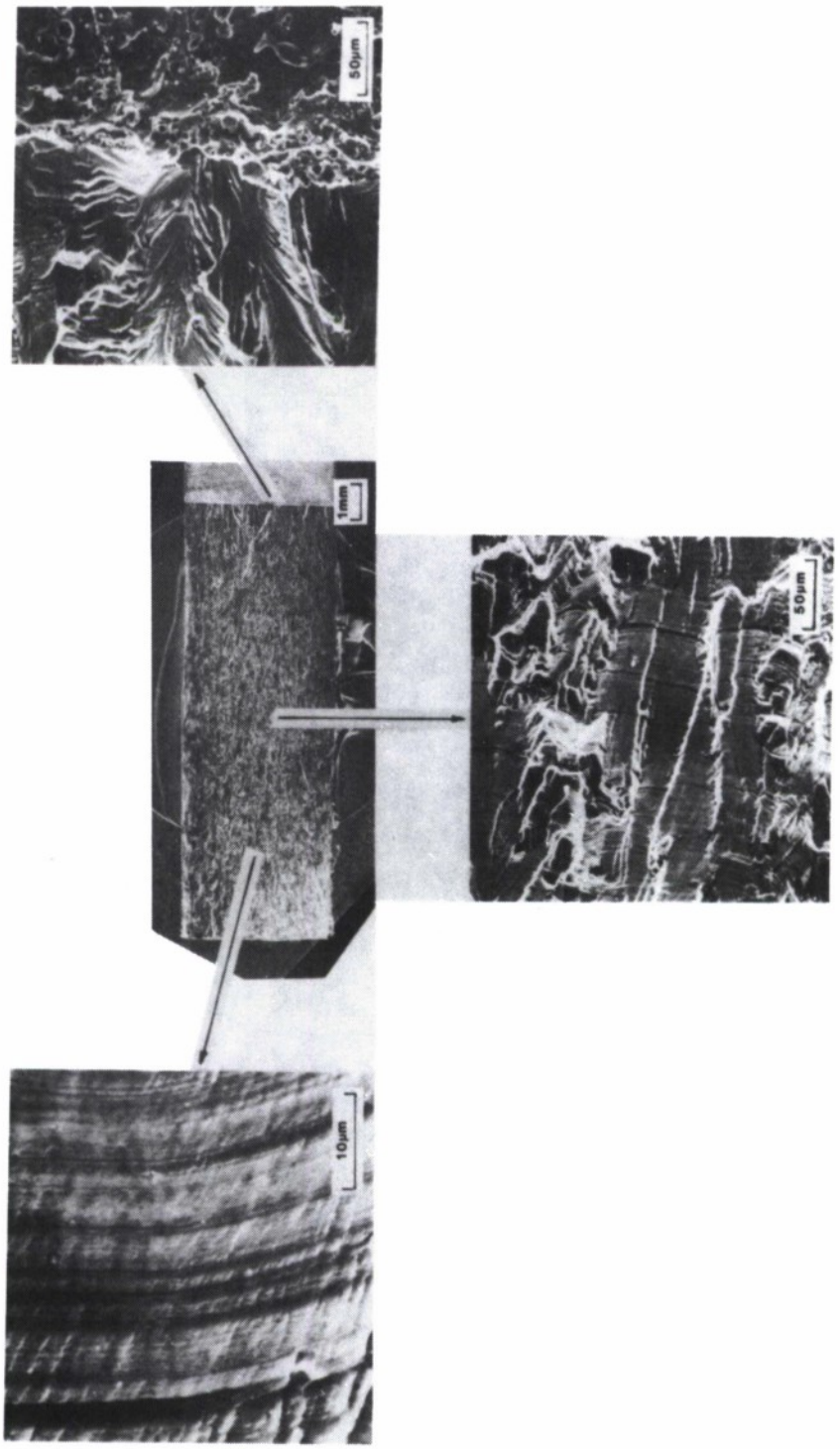

Figure 29. SEM Fractographs of I/M 7475-T7351 Aluminum Alloy, Fatigue-Tested under FALSTAFF Spectrum Loading.

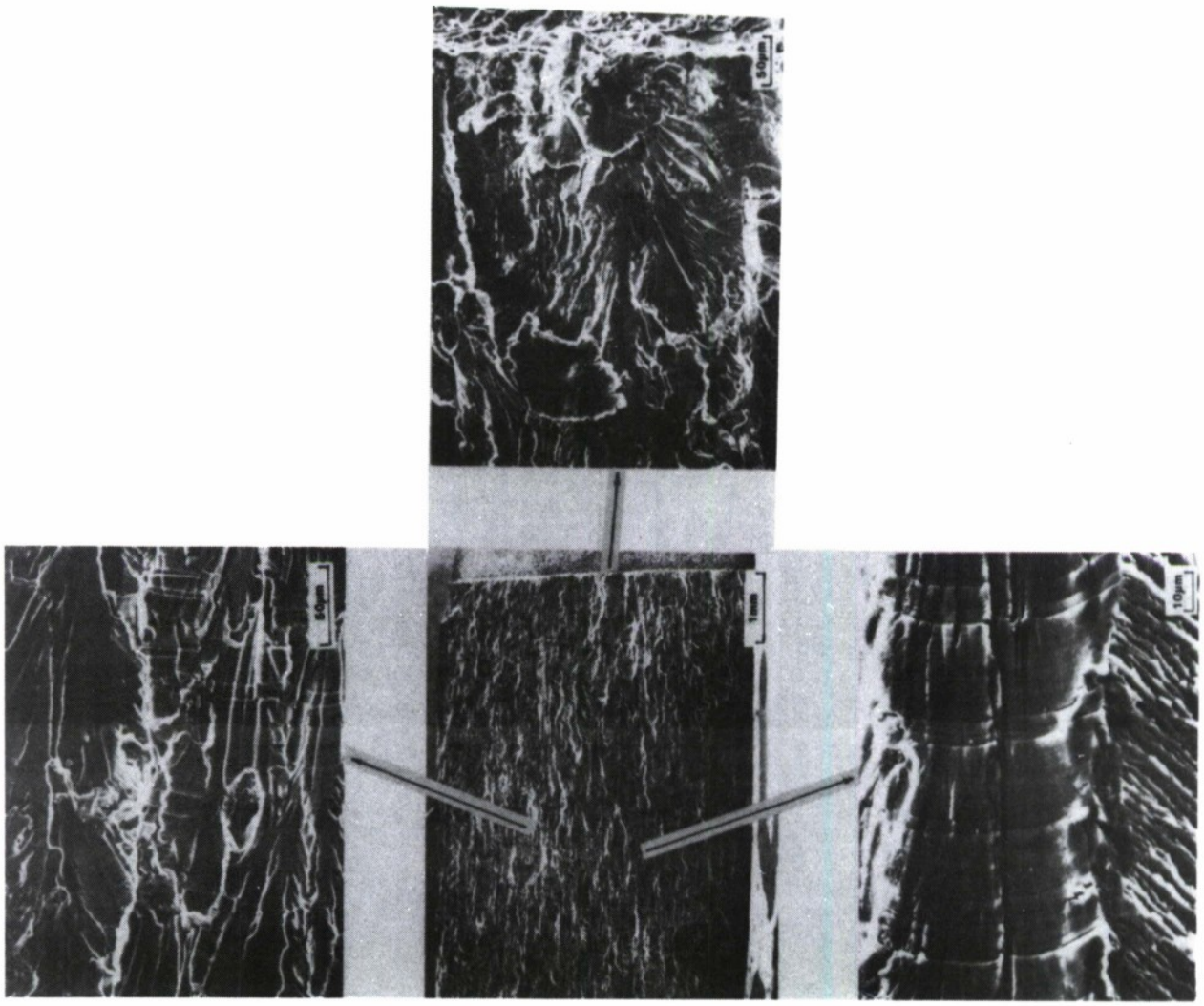

Figure 30. SEM Fractographs of I/M 7475-T7351 Aluminum Alloy, Fatigue-Tested under MINI-TWIST Spectrum Loading.

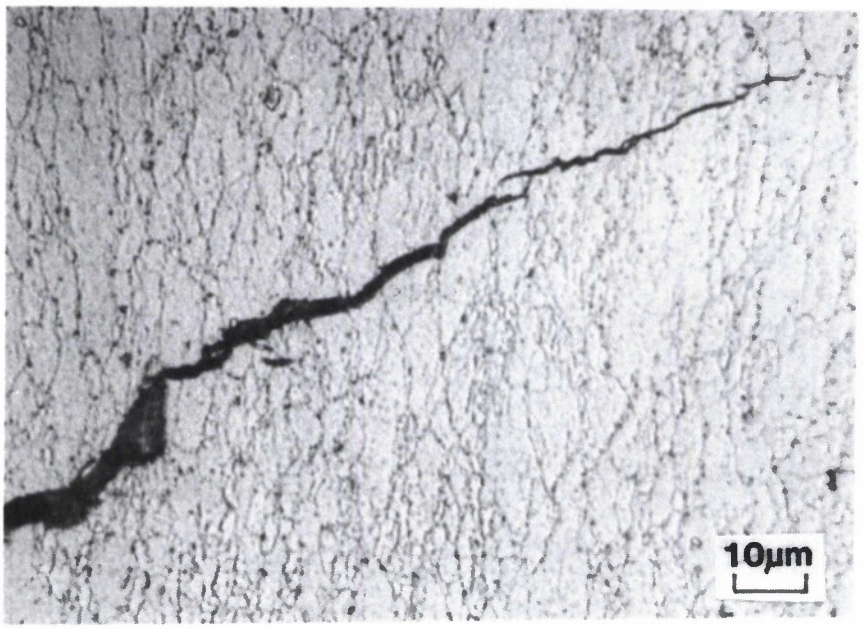

NOTE: This specimen was fatigue-tested under constant-amplitude loading with R=0.5. The specimen surface was polished and etched with Keller's reagent.

Figure 31. Deflection of Fatigue Crack Growth Path in P/M 7091-T7E69 Aluminum Alloy.

Table 1. Chemical Compositions of P/M 7091 and I/M 7475 Aluminum Alloys

Element	7091	7475
Zn	5.8 – 7.1	5.2 – 6.2
Mg	2.0 – 3.0	1.9 –2.6
Cu	1.1 – 1.8	1.2 – 1.9
Mn	—	0.06 max.
Cr	—	0.18 – 0.25
Co	0.2 – 0.6	—
Si	0.12 max.	0.10 max.
Fe	0.15 max.	0.12 max.
Ti	—	0.06 max.
Al	remainder	remainder

Table 2. Tensile Properties of P/M 7091–T7E69 Aluminum Alloy

0.2% Offset Tensile Yield Strength

	Loading Direction					
	L		T		ST	
Specimen No.	(ksi)	(MPa)	(ksi)	(MPa)	(ksi)	(MPa)
1	75.4	520.2	75.0	516.8	69.2	477.0
2	76.5	527.7	73.9	510.1	73.6	507.5
3	—	—	73.3	505.5	—	—
Ave. Value	76.0	524.0	74.1	510.8	71.4	492.3

Ultimate Tensile Strength

	Loading Direction					
	L		T		ST	
Specimen No.	(ksi)	(MPa)	(ksi)	(MPa)	(ksi)	(MPa)
1	80.7	556.3	81.6	562.5	78.5	541.7
2	82.6	569.5	79.7	549.8	79.9	550.7
3	—	—	80.3	553.7	—	—
Ave. Value	81.7	562.9	80.5	555.3	79.2	546.2

Elongation (%)

	Loading Direction		
Specimen No.	L	T	ST
1	12.0	9.0	10.2
2	11.5	10.0	11.5
3	—	8.0	—
Ave. Value	11.8	9.0	10.9

Table 3. Tensile Properties of I/M 7475–T7351 Aluminum Alloy

0.2% Offset Tensile Yield Strength

	Loading Direction			
	L		T	
Specimen No.	(ksi)	(MPa)	(ksi)	(MPa)
1	64.0	441.4	62.5	430.9
2	63.7	439.3	61.4	423.4
3	63.8	439.7	62.7	432.4
4	63.6	438.3	63.6	438.7
5	63.4	436.9	63.5	438.0
6	63.9	440.6	63.0	434.3
Ave. Value	63.7	439.4	62.8	433.0

Ultimate Tensile Strength

	Loading Direction			
	L		T	
Specimen No.	(ksi)	(MPa)	(ksi)	(MPa)
1	73.0	503.1	73.1	504.2
2	73.1	504.3	73.1	504.2
3	72.7	501.1	73.0	503.1
4	73.2	504.7	74.3	512.2
5	73.5	506.5	73.6	507.8
6	72.9	502.5	73.1	503.9
Ave. Value	73.1	503.7	73.4	505.9

Table 3. Tensile Properties of I/M 7475-T7351 Aluminum Alloy (Cont'd)

Elongation (%)

	Loading Direction	
Specimen No.	L	T
1	15.0	12.5
2	12.5	12.5
3	13.0	12.5
4	14.0	12.5
5	12.5	12.5
6	15.0	12.0
Ave. Value	13.7	12.4

Table 4. Fatigue Crack Growth Life under Constant Amplitude Loading

Material	Fatigue Crack Growth Life, N_f (cycle)			
	R = 0.1		R = 0.5	
	Individual	Mean	Individual	Mean
P/M 7091-T7E69	93,362	93,362	211,947	189,292
			166,637	
I/M 7475-T7351	508,327	486,694	720,669	720,669
	465,061			

Table 5. Fatigue Crack Growth Life under Aircraft Spectrum Loading

Material/Spectrum	Fatigue Crack Growth Life, N_f (No. of Flights)		
	FALSTAFF		MINI-TWIST
	Individual	Mean	Individual
P/M 7091-T7E69	33	88	1,465
	143		
I/M 7475-T7351	7,638		31,360

Table 6. Fracture Toughness Value, K_Q, (MPa$\sqrt{m}$)

Material	Specimen Orientation		Ref.
	LT	TL	
7091-T7E69	30.0	32.3	6
7475-T7351	53.7	41.7	16

DISTRIBUTION LIST

REPORT NO. NADC-89090-60

No. of Copies

Naval Air Development Center 22
Warminster, PA 18974-5000
(20 for Code 6063)
(2 for Code 8133)

Annapolis Laboratory 1
David W. Taylor Naval Ship Research and
Development Center Detachment
Annapolis, MD 21402-1198

Naval Aviation Depot 1
Naval Air Station
Code 340
Alameda, CA 94501-5201

Naval Aviation Depot 1
Marine Corps Air Station
Code 340
Cherry Point, NC 28533-5030

Naval Aviation Depot 1
Naval Air Station
Code 340
Jacksonville, FL 32212

Naval Aviation Depot 1
Naval Air Station
Code 340
Norfolk, VA 23511-5899

Naval Aviation Depot 1
North Island
Code 340
Pensacola, FL 32508-5300

Naval Aviation Depot 1
Naval Air Station
Code 340
San Diego, CA 92135-5112

Naval Post Graduate School 1
Monterey, CA 93940
Attn: Dr. E. R. Wood (Code 67)

DISTRIBUTION LIST

REPORT NO. NADC-89090-60

No. of Copies

Naval Air Systems Command 6
Washington, DC 20361-3030
(2 for AIR-530)
(2 for AIR-931A)
(1 for AIR-5302)
(1 for AIR-5304)

Naval Sea Systems Command 1
Washington, DC 20362

Naval Air Test Center 1
Patuxent River, MD 20670-5304

Naval Safety Center 1
NAS, Norfolk, VA 23511

Naval Research Laboratory 1
4555 Overlook Ave., SW
Washington, DC 20375

David W. Taylor Naval Ship Research and Development Center 1
Bethesda, MD 20084-5000

U.S. Air Force Systems Command 7
Wright-Patterson AFB, OH 45433
(1 for FBR)
(1 for FB)
(1 for LLD)
(1 for FYA)
(1 for LAM)
(1 for FBA)
(1 for LPH)

Chief of Naval Research 1
800 N. Quincy St.
Arlington, VA 22217-5000

Defense Technical Information Center 2
ATTN: DTIC-FDAB
Cameron Station BG5
Alexandria, VA 22304-6145

Center for Naval Analysis 1
4401 Fort Avenue
P.O. Box 16268
Alexandria, VA 22302-0268